Journal of Ethnopharmacology 335 (2024) 118689

Contents lists available at ScienceDirect

Journal of Ethnopharmacology

journal homepage: www.elsevier.com/locate/jethpharm

Unveiling the antitumor mechanism of 7α-acetoxy-6β-hydroxyroyleanone from Plectranthus hadiensis in glioblastoma

Mariana Magalhães [a,b,c,d], Eva María Domínguez-Martín [e,f], Joana Jorge [g,h], Ana Cristina Gonçalves [g,h], Francesca Massenzio [i], Renato Spigarelli [j], Teresa Ribeiro-Rodrigues [b,c,d], Steve Catarino [c,d], Henrique Girão [c,d], Barbara Monti [i], Enzo Spisni [j], Lino Ferreira [b,d,k], Paulo J. Oliveira [b,d], Thomas Efferth [l], Patrícia Rijo [e,m], Célia Cabral [c,d,n,*]

[a] University of Coimbra, Institute for Interdisciplinary Research, Doctoral Programme in Experimental Biology and Biomedicine (PDBEB), Portugal
[b] University of Coimbra, CNC—Center for Neuroscience and Cell Biology, Coimbra, Portugal
[c] University of Coimbra, Coimbra Institute for Clinical and Biomedical Research (iCBR), Clinic Academic Center of Coimbra (CACC), Faculty of Medicine, Coimbra, Portugal
[d] University of Coimbra, Center for Innovative Biomedicine and Biotechnology (CIBB), Coimbra, Portugal
[e] CBIOS—Universidade Lusófona's Research Center for Biosciences & Health Technologies, Lisbon, Portugal
[f] Departamento de Ciencias Biomédicas, Facultad de Farmacia, Universidad de Alcalá de Henares, Madrid, Spain
[g] University of Coimbra, Laboratory of Oncobiology and Hematology, University Clinic of Hematology and Applied Molecular Biology, Faculty of Medicine, Coimbra, Portugal
[h] University of Coimbra, ICBR, Group of Environment Genetics and Oncobiology (CIMAGO)—Faculty of Medicine, Coimbra, Portugal
[i] Department of Pharmacy and Biotechnology, University of Bologna, Bologna, Italy
[j] Department of Biological, Geological and Environmental Sciences, University of Bologna, Bologna, Italy
[k] University of Coimbra, Faculty of Medicine, Coimbra, Portugal
[l] Department of Pharmaceutical Biology, Institute of Pharmaceutical and Biomedical Sciences, Johannes Gutenberg University, Mainz, Germany
[m] Faculty of Pharmacy, Instituto de Investigação Do Medicamento (iMed.ULisboa), University of Lisbon, Lisbon, Portugal
[n] University of Coimbra, Centre for Functional Ecology, Department of Life Sciences, Coimbra, Portugal

ARTICLE INFO

Handling Editor: V Kuete

Keywords:
Glioblastoma
Plectranthus hadiensis schweinf.
Royleanone
Abietane diterpenes
Antitumor activity

ABSTRACT

Ethnopharmacological relevance: Glioblastoma (GB) is the most aggressive and prevalent glioma within the central nervous system. Despite considerable efforts, GB continues to exhibit a dismal 5-year survival rate (~6%). This is largely attributed to unfavorable prognosis and lack of viable treatment options. Therefore, novel therapies centered around plant-derived compounds emerge as a compelling avenue to enhance patient survival and well-being. The South African species, *Plectranthus hadiensis* Schweinf. (*P. hadiensis*), a member of the Lamiaceae family, has a history of use in traditional medicine for treating a range of diseases, including respiratory, digestive, and liver disorders. This species exhibits diverse biological activities, such as anti-inflammatory and antitumoral properties, likely attributed to its rich composition of naturally occurring diterpenes, like the abietane diterpene, 7α-acetoxy-6β-hydroxyroyleanone (Roy). Roy has demonstrated promising antitumor effects in various cancer cell lines, making it a compelling candidate for further investigation into its mechanisms against GB.

Aim of the study: This study aims to investigate the antitumor activity and potential mechanism of Roy, a natural lead compound, in GB cells.

Material and methods: Roy was isolated from the acetonic extract of *P. hadiensis* and its antitumor mechanism was assessed in a panel of human GB cell lines (U87, A172, H4, U373, and U118) to mimic tumor heterogeneity. Briefly, the impact of Roy treatment on the metabolic activity of cells was evaluated by Alamar Blue® assay, while cell death, cell cycle regulation, mitochondrial membrane potential, and activated caspase-3 activity were evaluated by flow cytometry. Measurement of mRNA levels of target genes was performed by qPCR, while protein expression was assessed by Western blotting. Cell uptake and impact on mitochondrial morphology were evaluated by confocal microscopy.

* Corresponding author. Faculty of Medicine, University of Coimbra, Pólo das Ciências da Saúde, Azinhaga de Santa Comba, 3000-548, Coimbra, Portugal.
E-mail address: celia.cabral@fmed.uc.pt (C. Cabral).

https://doi.org/10.1016/j.jep.2024.118689
Received 12 June 2024; Received in revised form 30 July 2024; Accepted 9 August 2024
Available online 14 August 2024

Results: Roy induced G_2/M cell cycle arrest, mitochondrial fragmentation, and apoptosis by inhibiting the expression of anti-apoptotic proteins and increasing the levels of activated caspase-3. The concentrations of Roy needed to achieve significant inhibitory outcomes were notably lower (6–9 fold) than those of temozolomide (TMZ), the standard first-line treatment, for achieving comparable effects. In addition, at low concentrations (16 μM), Roy affected the metabolic activity of tumor cells while having no significant impact on non-tumoral cells (microglia and astrocytes).
Conclusion: Overall, Roy demonstrated a robust antitumor activity against GB cells offering a promising avenue for the development of novel chemotherapeutic approaches.

Abbreviations

GB	Glioblastoma
CNS	Central nervous system
WHO	World health organization
TMZ	Temozolomide
MDR	Multidrug resistance
MGMT	O6-methylguanine-DNA methyltransferase
Roy	7α-acetoxy-6β-hydroxyroyleanone
P. hadiensis	Plectranthus hadiensis Schweinf
NMR	Nuclear magnetic resonance
DCM	Methylene chloride
HCL	Hydrochloric acid (HCL)
EDC	1-[3-(dimethylamino)propyl]-3-ethylcarbodiimide methiodide
DMAP	4-(Dimethylamino)pyridine
DMEM-HG	Dulbecco's Modified Eagle's Medium-high glucose
FBS	Fetal bovine serum
BME	Basal medium eagle
MTT	3-(4,5-dimethylthiazol-2-yl)-2,5-diphenyl tetrazolium bromide
IC50	Half-maximal inhibitory concentration
PI	Propidium iodide
AV	Annexin V
JC-1	5,5,6,6′-tetrachloro-1,1′,3,3′ tetraethylbenzimidazoylcarbocyanine iodide
BCL2	B-cell lymphoma-2
BCL2l1	Bcl-2-like protein 1
CASP9	Caspase 9
PTEN	Phosphatase and tensin homolog
TP53	Tumor protein p53 (TP53)
PARP1	Poly(ADP-ribose) polymerase 1
MDM2	Murine double minute 2
BCA	Bicinchoninic acid assay
FITC	Fluorescein isothiocyanate
MFI	Mean fluorescence intensity
PI3K	Phosphatidylinositol 3-kinase
Akt	Protein kinase B
FF	Form factor
AR	Aspect ratio

1. Introduction

Glioblastoma (GB), the most common and malignant primary glioma of the central nervous system (CNS), encompassing brain and spinal cord tumors, is classified by the World Health Organization (WHO) as a grade 4 adult-type diffuse glioma (Louis et al., 2021). This highly aggressive and lethal glioma continues to create significant challenges to medicine and patient care. Characterized by rapid growth and high invasiveness, this devastating disease has a dismal prognosis, with a median survival of approximately 15–18 months post-diagnosis even with treatment (Wen and Packer, 2021). This is primarily attributed to the infiltrative behavior and localization of the tumor, as well as, to the extent of surgery and treatment resistance (Hazaymeh et al., 2022; Kow et al., 2020; Tan et al., 2020). The established treatment protocol for GB patients involves surgical resection followed by cycles of chemoradiotherapy and adjuvant chemotherapy (temozolomide-TMZ) (Angom et al., 2023; Rončević et al., 2023). TMZ is an alkylating agent that disrupts DNA chains by adding a methyl group to guanine, acting on DNA replication and leading to the activation of pathways involved in apoptosis (Chien et al., 2021; Ortiz et al., 2021). However, these treatments have limitations, including incomplete tumor resection and the emergence of multidrug resistance (MDR) linked to TMZ therapy, through the activity of O6-methylguanine-DNA methyltransferase (MGMT) and the presence of gene mutations that conduct a permanent activation of multiple survival pathways, contributing to tumor recurrence (Angom et al., 2023; Ortiz et al., 2021; Rončević et al., 2023). As a result, the ongoing quest for more effective and targeted GB therapies persists, with emerging interest in novel treatments centered on molecules with natural origin. This interest is fueled by the inherent chemical diversity and pharmacological potency of such compounds, which underlie the historical significance of plants as vital sources of medicines (Howes, 2018; Rodrigues et al., 2016).

In traditional medicine, plants are extensively used to address the treatment of various illnesses and serve as a rich source of bioactive compounds with considerable therapeutic potential, such as anti-inflammatory, antioxidant, antiproliferative, and antitumor activity (Domínguez-Martín et al., 2023; Howes, 2018; Rayan et al., 2017). The unique chemical structure of natural bioactive compounds with distinct mechanisms of action against complex diseases such as cancer, position them as fundamental contributors in the quest for novel and more effective anticancer drugs (Howes, 2018). Terpenes are a well-known category of secondary metabolites, recognized for their established chemopreventive and chemotherapeutic properties (e.g., paclitaxel, the active substance from Taxol®, a clinically employed anticancer drug for ovarian and breast cancer treatment) (Domínguez-Martín et al., 2023; Howes, 2018; Yang et al., 2020).

The genus *Plectranthus* L'Hér. represents a rich source of abietane diterpenes, a class of compounds responsible for diverse and appealing therapeutic bioactivities (Bangay et al., 2024; Domínguez-Martín et al., 2023). One of these abietane diterpenes is 7α-acetoxy-6β-hydroxyr oyleanone (Roy), which is isolated from *Plectranthus hadiensis* Schweinf. (*P. hadiensis*) (Domínguez-Martín et al., 2022; Sitarek et al., 2020; Śliwiński et al., 2020). Roy has garnered considerable interest due to its reported antitumor potential *in silico* and *in vitro* against several cancer cell lines (Isca et al., 2024; Merecz-Sadowska et al., 2024; Sitarek et al., 2020; Śliwiński et al., 2020). The investigation and repurposing of Roy as a potential natural lead compound for GB offers a novel avenue for treatment that may complement existing therapies or serve as a basis for the development of novel therapeutic approaches.

In this study, our objective is to investigate the antitumor effect of Roy as a potential GB treatment. Previously, we assessed the cytotoxic

effect of Roy on a panel of different GB cell lines (Domínguez-Martín et al., 2022), to cover the distinct molecular subtypes and heterogeneity of this tumor, shedding light on its potential antitumor activity. Here, we unveiled the mechanism of action, cytotoxic and pro-apoptotic profile of Roy in GB cells.

2. Materials and methods

2.1. Plant material

P. hadiensis was grown in Parque Botânico da Tapada da Ajuda (Lisbon, Portugal) and provided by the Kirstenbosch National Botanical Gardens (Kirstenbosch, South Africa). The voucher specimens 833/2007 and 438/2010 were deposited in the herbarium *João de Carvalho e Vasconcellos* of the Instituto Superior de Agronomia (Lisbon, Portugal). The plant was air-dried at room temperature and stored in cardboard boxes protected from light and humidity to maintain its stability (Domínguez-Martín et al., 2022).

2.2. Isolation of roy

The abietane diterpene Roy (Fig. 1) was isolated from the acetonic extract of *P. hadiensis* leaves, as previously described (Domínguez-Martín et al., 2022; Ntungwe et al., 2021). Roy was then purified by dry-column flash-chromatography, using silica as a stationary phase and a gradient of eluents of increasing polarity (n-Hexane:Ethyl acetate) as a mobile phase. Roy structure was elucidated through nuclear magnetic resonance (NMR) spectra assignments and previously published (Ntungwe et al., 2021).

2.3. Synthesis of Roy-BODIPY

Roy-Bodipy was synthesized following the protocol previously described (Domínguez-Martín et al., 2022). Briefly, succinic anhydride was added to a mixture of BODIPY (fluorescent probe) and triethylamine in anhydrous dichloromethane. The reaction mixture was stirred at room temperature. The solution was diluted with methylene chloride (DCM) and aqueous hydrochloric acid (HCL) (1M) until reach pH 3. The resulting mixture was washed with H_2O, the layers were separated, and the organic layer was washed with brine, dried, and concentrated. The crude material of succinimidyl-modified BODIPY was employed in the subsequent stage without undergoing additional purification (88%). A mixture of carboxylic acid (succinimidyl-modified BODIPY) and abietane in anhydrous dichloromethane was cooled to 0 °C and treated under argon atmosphere with 1-[3-(dimethylamino)propyl]-3-ethylcarbodiimide methiodide (EDC) and a catalytic amount of 4-(Dimethylamino)pyridine (DMAP). The reaction mixture was stirred for 90 min. The solution was diluted with DCM and washed with H_2O. The layers were separated, and the organic layer was dried and concentrated. The crude material was purified through silica column chromatography to yield Roy-BODIPY (65%). NMR data regarding Roy-Bodipy structure was previously published by our group (Domínguez-Martín et al., 2022).

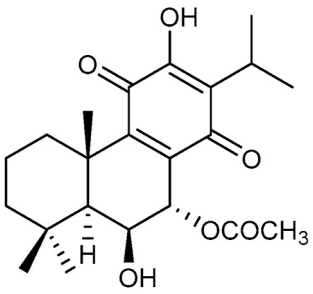

Fig. 1. Chemical structure of 7α-acetoxy-6β-hydroxyroyleanone (Roy).

2.4. Cell culture

In order to cover GB heterogeneity, a panel of 5-glioma human cell lines, U87, A172, H4, U373, and U118, was used. All cell lines used in this work were acquired from the American Type Culture Collection (ATCC).

U87 (brain-likely GB, ATCC HTB-14), A172 (GB, ATCC CRL-1620), and H4 (neuroglioma, ATCC HTB-148) cell lines were provided by Prof. Carla Vitorino (Faculty of Pharmacy, University of Coimbra), while U118 (astrocytoma/GB, ATCC HTB-15) and U373 (astrocytoma/GB, ATCC HTB-17) cell lines were provided by Prof. Maria Conceição Pedroso de Lima (Faculty of Sciences and Technology/Center for Neuroscience and Cell Biology, University of Coimbra). The HMC3 (human microglia, ATCC CRL-3304) cell line was provided by Prof. Célia Gomes (Coimbra Institute for Clinical and Biomedical Research (iCBR), Faculty of Medicine, University of Coimbra). Cells were grown in Dulbecco's Modified Eagle's Medium-high glucose (DMEM-HG) (Biowest, Nuaillé, France) supplemented with 10% (v/v) of heat-inactivated fetal bovine serum (FBS) (Biowest, Nuaillé, France) and 1% (v/v) of penicillin-streptomycin (Sigma, St. Louis, MO, United States), being maintained at 37 °C, 5% CO_2, and 95% of humidity. All cells were used until a maximum of 10 passages counting from the initial vial. All experiments were performed in cultures in log phase growth. Cells were subcultured by trypsinization, except for U118 cells that were subcultured using a scrapper, when reaching 80–90 % confluence. Cell density for each experiment was optimized at the beginning of each assay using growth curves.

2.5. Primary rat culture of astrocytes

Primary cultures of astrocyte-enriched cells were obtained from mixed glial cultures, which were isolated from the cerebral cortex of newborn Wistar rats, as previously described (Massenzio et al., 2018). All animal experiments were authorized by the bioethical committee (Protocol n° 1088/2020) and performed in agreement with the Italian and European Community laws on the use of animals for experimental purposes. Briefly, cerebral cortices were collected and cleared of meninges, trypsinized, and mechanically dissected. Cell suspensions were resuspended in Basal Medium Eagle (BME; Life Technologies Italia, Monza, Italy) with 10% (v/v) heat-inactivated FBS (Life Technologies), 2 mM glutamine (Sigma, St. Louis, MO, USA), and 100 μM gentamicin sulfate (Sigma, St. Louis, MO, USA) and plated on flasks previously coated with poly-l-lysine (10 μg/ml; Sigma, St. Louis, MO, USA). One week later, microglial cells were harvested from mixed glial cell cultures by mechanical shaking and discarded to obtain a primary culture of astrocyte cells.

2.6. 3-(4,5-Dimethylthiazol-2-yl)-2,5-diphenyl tetrazolium bromide (MTT) assay

3-(4,5-dimethylthiazol-2-yl)-2,5-diphenyl tetrazolium bromide (MTT) assay was used in this work to assess the cytotoxic/anti-proliferative effect of Roy in primary astrocyte cells, once it is the standard operation protocol (SOP) in the laboratories of Prof. Spisni and Prof. Monti at the University of Bologna, being widely accepted as a reliable methodology to measure metabolic activity and proliferation of cells.

Primary astrocyte cells (2×10^4 cells/well) were seeded in 96-well plates. After 1 h, cells were treated with a range of Roy concentrations (1–64 μM) and further incubated for 24 h. Thereafter, cells were incubated with 3-(4,5-dimethylthiazol-2-yl)-2,5-diphenyl tetrazolium bromide (MTT) (Sigma, St. Louis, MO, USA), at a concentration of 0.1 mg/ml. After 45 min, MTT was carefully removed and 0.1 mol/l of Tris-HCl buffer containing 5% Triton X-100 (Sigma, St. Louis, MO, USA) was added to each well. Absorbance was measured at 570 nm in a Multiplate Spectophotometric Reader (Bio-Rad, CA, USA) (Polazzi et al., 2009).

Metabolic activity was expressed as a percentage of control (untreated cells).

2.7. Alamar Blue® assay

Alamar Blue® assay is a well-established protocol in our group, being a simple and low-cost method with high sensitivity and widely used to measure the reducing environment and metabolic activity of cells. In this work, it was used as a preliminary assay to measure the cytotoxic/antiproliferative activity of Roy in GB cells in comparison with the standard first-line treatment (TMZ), while also assessing its potential tumor-specific effect in non-tumoral cells (microglia cell line).

U87, A172, H4, U373, U118 cells (1×10^4 cells/well), and HMC3 cells (2×10^4 cells/well) were seeded in 96-well plates, 24 h before treatment. Cells were treated with a range of Roy concentrations (1–64 μM), with the vehicle control (DMSO), or with positive control (TMZ – 1 to 100 μM), and further incubated for 48 h. Metabolic activity was assessed through Alamar Blue® assay (Magalhães et al., 2014). Briefly, a solution of DMEM-HG medium with 10% (v/v) of a resazurin salt dye stock solution (Sigma. St. Louis, MO, United States) at a 0.1 mg/ml concentration was prepared and added to each well after the 48 h treatment. After 4 h of incubation at 37 °C and 5% CO_2, as previously optimized for these cell lines, the absorbance of each sample was read at 570 and 600 nm using a BioTeck Synergy HT microplate reader (BioTek Instruments, Inc., Winooski, VT, United States) and Gen5 software. Metabolic activity was obtained in accordance with the following equation:

$$\textit{Metabolic activity}\ (\%) = \frac{(A570 - A600)\ \textit{of treated cells}}{(A570 - A600)\ \textit{of control cells}} \times 100$$

Half-maximal inhibitory concentration (IC_{50}) values were further calculated using GraphPad Prism Software v.10.1.0 (GraphPad Software, Inc.) (Magalhães et al., 2022).

2.8. Cell cycle

The impact of Roy on cell cycle was analyzed by flow cytometry using propidium iodide (PI)/RNase solution, according to the manufacturer's protocol (Immunostep, Salamanca, Spain), and as previously described (Alves et al., 2019), as it is a simple, easy, fast, and highly sensitive methodology to reveal useful information on cell cycle regulation, relative to other methodologies, as PI stains DNA and RNA is removed by digestion with RNase. Briefly, U87, A172, H4, U373, and U118 cells were seeded with a density of 30×10^4 cells/well in a 6-well plate. After 24 h, cells were treated with 16 μM of Roy and further incubated during 48 h. Cells were detached, fixed in 70% ethanol for 60 min at 4 °C, washed twice with PBS, and then stained with 500 μl PI/RNase solution. Cell cycle distribution was analyzed using the ModFit LT software (Verity Software House). Results were acquired using CellQuest software and expressed in percentage of cells in the different cell cycle phases (G_0/G_1, S, and G_2/M) according to the PI intensity. A sub-G_1 population was also identified corresponding to apoptotic cells.

2.9. Cell death assay

Cell death was measured using the Annexin V (AV)/PI assay by flow cytometry, a well-established methodology in our laboratory that allows a simple and fast way to distinguish among viable cells, cells in early apoptosis, and cells in late apoptosis or necrosis upon treatment, as previously described (Magalhães et al., 2022). Briefly, 24 h before treatment, U87, A172, H4, U373, and U118 cells (20×10^4 cells per well) were seeded in 12-well plates. The cell medium was replaced, and the cells were treated with Roy (16 μM). After 48 h, cells were co-stained with AV-APC and PI according to the manufacturer's protocol (Biolegend, San Diego, CA, USA). Cells were resuspended in binding buffer (100 μl) and incubated with AV-APC solution (5 μl) and PI solution (2 μl). A six-parameter, four-color FACSCalibur flow cytometer (Becton Dickinson, San Jose, CA, USA) was used and at least 10.000 events were collected by acquisition using CellQuest software (Becton Dickinson, San Jose, CA). The results were analyzed with the Paint-a-Gate software and were expressed in percentage (%). Viable cells were negative for AV and PI staining (AV-/PI-), cells in early apoptosis were positive for AV staining (AV+/PI−), cells in necrosis were positive for PI staining (AV−/PI+), and cells in late apoptosis/necrosis were positive for AV and PI staining (AV+/PI+).

2.10. Mitochondrial membrane potential

Mitochondrial membrane potential (ψmit) was indirectly measured using 5,5,6,6′-tetrachloro-1,1′,3,3′ tetraethylbenzimi-dazoylcarbo cyanine iodide (JC-1) (Enzo Life Sciences, Farmingdale, NY, USA), a membrane-permeant dye widely used to assess mitochondria health in studies to evaluate apoptosis using several cell types, as previously described (Gonçalves et al., 2013). Briefly, U87, A172, H4, U373, and U118 cells were seeded with a density of 30×10^4 cells/well in a 6-well plate. After 24 h, cells were treated with 16 μM of Roy and further incubated for 48 h. After incubation, cells were washed twice with PBS, centrifuged, and incubated with JC-1 at a final concentration of 5 μg/ml for 15 min at 37 °C in the dark. Cells were washed twice with PBS, resuspended in a total volume of 500 μl, and analyzed by flow cytometry.

2.11. Quantitative real-time PCR

Quantitative real-time PCR (qRT-PCR) was used in this work to measure mRNA levels of genes involved in cell proliferation and apoptotic signaling pathways to better understand Roy's mechanism of action, as this is a rapid and sensitive technique to quantify changes in gene expression.

B-cell lymphoma-2 (*BCL2*), *Bcl-2-like protein 1* (*BCL2L1*), *caspase 9* (*CASP9*), *Phosphatase And Tensin Homolog* (*PTEN*), *tumor protein p53* (*TP53*), *Poly(ADP-Ribose) Polymerase 1* (*PARP1*), and *murine double minute 2* (*MDM2*) mRNA levels were quantified by qRT-PCR. Briefly, U87, A172, H4, U373, and U118 cells were seeded with a density of 1×10^6 cells per well 24 h before treatment. After, 16 μM of Roy was added to cells, which were further incubated for 48 h. Total RNA was extracted using TripleXtractor solution (GRISP, Lisbon, Portugal) according to the manufacturer's protocol. RNA was converted into cDNA through the Xpert cDNA Synthesis Supermix (GRISP, Lisbon, Portugal), following the manufacturer's protocol. 100 ng of cDNA was amplified by qRT-PCR using the primers in Table 1. Each optimized reaction was performed using Xpert Fast SYBR Green Mastermix 2X with ROX (GRISP, Lisbon, Portugal) and samples were subjected to the amplification protocol described by the manufacturer, using a melting temperature of 60 °C. Relative gene expression was determined by the $2^{-\Delta\Delta Ct}$ method and normalized to the *glyceraldehyde-3-phosphate dehydrogenase* (*GAPDH*) gene, the endogenous reference, and relative to the untreated control cells. Optimization conditions are described in Supplementary Table S1.

2.12. Western blotting

Western blotting is a widely used and recognized technique to detect a specific protein in a mixture from biological samples. In this work, this technique was used to measure the expression of specific proteins, involved in anti-apoptotic mechanisms, that are overexpressed in GB cells.

U87, A172, H4, U373, and U118 cells were seeded in 90 mm cell culture dishes, with a density of 1×10^6 cells per dish, and subjected to a treatment with 16 μM of Roy. After 48 h, cells were washed twice with PBS, detached mechanically, and resuspended in RIPA buffer (50 mM Tris, 150 mM NaCl, 1% NP-40, and 0.1% SDS in the presence of protease inhibitors). Cell lysates were centrifuged at 4 °C, 12000 RCF for 10 min,

Table 1
Sequence of the primers and respective concentration used, for each optimized reaction, in quantitative real-time PCR (qRT-PCR).

Gene	Primers concentration (nM)	Forward (5′-3′)	Reverse (5′-3′)
BCL2	100	GAGGATTGTGGCCTTCTTTGAG	AGCCTCCGTTATCCTGGATC
BCL2L1	150	GCCACTTACCTGAATGACCACC	AACCAGCGGTTGAAGCGTTCCT
PARP1	300	CGGAGTCTTCGGATAAGCTCT	TTTCCATCAAACATGGGCGAC
MDM2	150	TGTTTGGCGTGCCAAGCTTCTC	CACAGATGTACCTGAGTCCGATG
CASP9	150	GTTTGAGGACCTTCGACCAGCT	CAACGTACCAGGAGCCACTCTT
PTEN	100	TGAGTTCCCTCAGCCGTTACCT	GAGGTTTCCTCTGGTCCTGGTA
TP53	75	CAGCACATGACGGAGGTTGT	TCATCCAAATACTCCACACGC
GAPDH	150	GTCTCCTCTGACTTCAACAGCG	ACCACCCTGTTGCTGTAGCCAA

and protein content was measured using a bicinchoninic acid assay (BCA) kit (Thermo FisherScientific, Waltham, MA, USA). Equal amounts of total cell protein (30 μg) were separated by electrophoresis on SDS polyacrylamide gels (SDS-PAGE) and transferred to polyvinylidene difluoride (PVDF) membranes. Membranes were blocked with 5% non-fat milk in Tris-buffered saline with 0.1% Tween-20 (TBS-T) for 1h at room temperature, followed by incubation with the primary antibodies overnight at 4 °C. Membranes were washed with TBS-T and incubated with the secondary antibody. The antibodies used were anti-p21 (1:1000, ab7960, Abcam) and anti-Bcl-2 (1:1000, cs2870, Cell Signaling). Anti-β-actin (1:10000, A5441, Sigma) was used as loading control. Membranes were developed using ECL and ImageQuant imaging system (GE Healthcare, Chicago, IL, USA). The densitometric analysis of band intensity was performed using Image Lab software (Bio-Rad, CA, USA), and the values are presented relative to the loading control (β-actin).

2.13. Activated caspase-3 expression analysis

Activated caspase-3 expression levels were measured by flow cytometry using BD Pharmingen™ monoclonal antibody anti-activated caspase-3 labeled with fluorescein isothiocyanate (FITC) (BD Biosciences, Franklin Lakes, NJ, USA), according to the manufacturer's protocol. Briefly, U87, A172, H4, U373, and U118 cells were seeded at a density of 1×10^6 cells per well and each condition was treated with 16 μM of Roy for 48 h. Afterward, cells were fixed with BD Cytofix/Cytoperm™ solution for 20 min on ice and then washed by centrifugation at 3450 RPM for 5 min. Cells were then incubated with 20 μl of FITC rabbit anti-active caspase-3. After a 30-min incubation period at room temperature, the cells were washed and resuspended in 400 μl of PBS for flow cytometry analysis. At least 25,000 events were acquired using CellQuest software (Becton Dickinson, San Jose, CA, USA) and analyzed using Paint-a-Gate (Becton Dickinson, San Jose, CA, USA). The results are obtained as mean fluorescence intensity (MFI) arbitrary units, being MFI detected in the cells, which is proportional to the protein concentration in each cell and are presented as percentage (%) of positive cells.

2.14. Confocal microscopy

Live confocal fluorescent microscopy was used to visualize the internalization and distribution of Roy labeled with BODIPY in GB cells, as well as, the impact of this natural compound in mitochondria morphology. U87, A172, H4, U373, and U118 cells (15×10^4 cells/well) were seeded in μ-Dish 35 mm, polymer coverslip, ibiTreat (ibidi GmbH, Gräfelfing, Germany). After 24 h, cells were treated with 16 μM of Roy-BODIPY and further incubated during 48 h 30 min before the end of treatment, cells were incubated with 100 nM of MitoTracker Red FM (ThermoFisher Scientific, Waltham, MA, USA) and 1 μg/ml of Hoechst 33342 (ThermoFisher Scientific, Waltham, MA, USA) for mitochondrial network and nuclei, respectively, in the presence of serum-free medium and protected from light. Images were acquired using a laser scanning confocal inverted microscope (LSM 710 configured to an Axio Observer Z1 microscope, QUASAR detection unit, ZEN Black software (Carl Zeiss, Germany)) using a pinhole of 1 airy unit, a 63 × oil objective (Plan-Apochromat, 1.4 NA), and Diode 405–30 (405 nm), Argon/2 (488 nm) and DPSS 561–10 (561 nm) lasers. Images were analyzed with ImageJ software (Scion Corporation, USA). 2D analysis of the mitochondrial network morphological features was performed using Fiji/ImageJ software (NIH). The mean area and perimeter (representing the mitochondrial size) and the form factor (FF) and aspect ratio (AR) (representing the mitochondrial shape) were analyzed using the mitochondrial analyzer function from Fiji/ImageJ software (NIH) (Chaudhry et al., 2019).

2.15. Statistical analysis

Data were analyzed using GraphPad Prism v.10.1.0. All experiments are representative of at least three independent experiments and acquired results were expressed as mean ± standard deviation (SD). Statistical analysis was performed by using t-student test, one-way and two-way ANOVA, using the unpaired comparison and the Dunnett and Šidák multiple comparison tests, respectively. A value of $p < 0.05$ was considered significant.

3. Results

3.1. Roy effect in the metabolic activity of GB cells

Treatment with Roy significantly inhibited the metabolic activity of GB cells, being much more effective than TMZ, even at the highest concentration (100 μM was used taking into account the dose of TMZ used in the clinic (75 mg/m^2) (Clinic, 2024)) (Fig. 2). This result is further corroborated by the IC_{50} values outlined in Table 2. The cell lines U373 and U118 displayed higher sensitivity to the treatment, in comparison to U87, A172, and H4 cells. Across all cell lines, the concentrations of Roy required to achieve a 50% reduction in cell viability were notably lower than the corresponding TMZ concentrations (Table 2). Noteworthy, differences emerged in the IC_{50} values necessary to induce cell death: U118 (14.44 μM) and U373 (17.02 μM) cells exhibited IC_{50} values that were 15 and 24 times lower than the necessary TMZ concentration to induce the same effect (213.49 and 409.01 μM for U118 and U373 cells, respectively) (Table 2). Higher IC_{50} values were observed for Roy (59.37, 84.60, and 46.82 μM, respectively) in U87, A172, and H4 cells compared to U118 and U373 cells. Nevertheless, Roy still displayed superior efficacy, requiring concentrations around 6, 9, and 11 times lower than those of TMZ needed to achieve a 50% inhibition of proliferation in U87, H4, and A172 cells (371.21, 444.91, and 948.39 μM, respectively) (Table 2).

Moreover, at a lower concentration (16 μM), Roy affected the metabolic activity of tumoral cells, while having no significant impact on non-tumoral cells (microglia cell line and primary astrocyte cells) (Figs. 3 and 4). For further studies, a treatment with 16 μM of Roy was administered to GB cells to explore this compound antitumoral mechanism of action.

3.2. Roy effect in cell viability of GB cells

The findings from metabolic activity assessments indicate that Roy exhibits a greater therapeutic potential against GB cells compared to

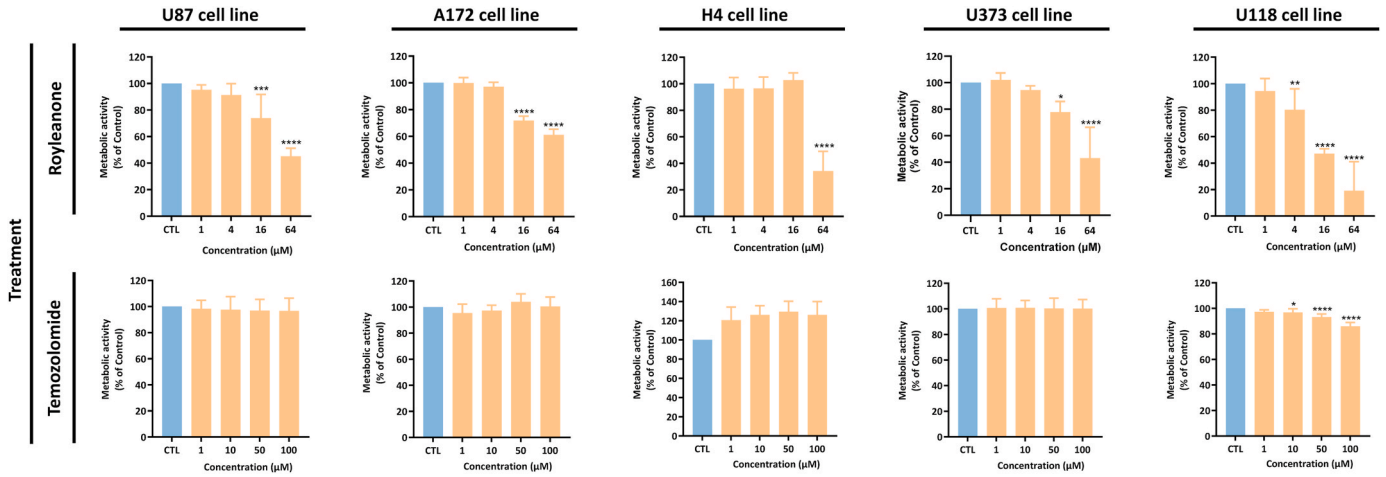

Fig. 2. Impact of Roy on the metabolic activity of glioblastoma cell lines. **A)** U87, A172, H4, U373, and U118 cells were treated either with Roy (1, 4, 16, and 64 μM) or with temozolomide (1, 10, 50, and 100 μM) for 48 h, and subsequently Alamar blue® assay was performed. Metabolic activity was expressed as percentage of control (CTL) (untreated cells). Asterisks (*$p < 0.05$, **$p < 0.01$, ***$p < 0.001$, and ****$p < 0.0001$) represent the values that significantly differ from the control. Data are representative of three independent experiments and are expressed as mean ± SD. (For interpretation of the references to color in this figure legend, the reader is referred to the Web version of this article.)

Table 2
Half-maximal inhibitory concentration (IC_{50}) values for Roy and TMZ in a panel of glioblastoma cell lines.

Compound	IC_{50} (μM)				
	U87 cell line	A172 cell line	H4 cell line	U373 cell line	U118 cell line
Roy	59.37	84.60	46.82	17.02	14.44
TMZ	371.21	948.39	444.91	409.01	213.49

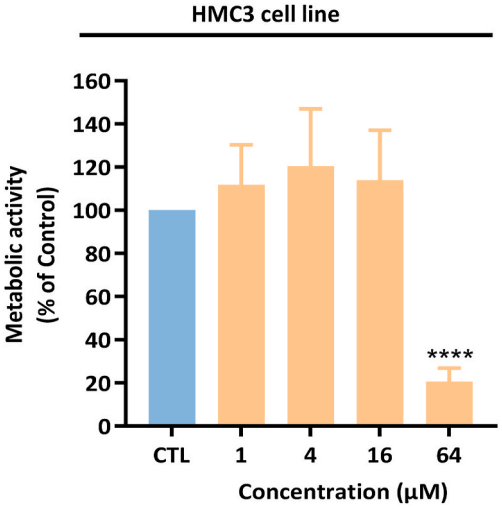

Fig. 3. Impact of Roy on the metabolic activity of microglia cells. HMC3 cell line was treated with Roy (1, 4, 16, and 64 μM) for 48 h and Alamar Blue® assay was performed. Metabolic activity was expressed as percentage of control (CTL) (untreated cells). Asterisks (****$p < 0.0001$) represent the values that significantly differ from the control. Data are representative of three independent experiments and are expressed as mean ± SD. (For interpretation of the references to color in this figure legend, the reader is referred to the Web version of this article.)

TMZ, the primary first-line treatment. This discovery suggests a promising initial step towards overcoming the challenges associated with TMZ treatment. Subsequently, we delved into the mechanism of cell death in tumoral cells using AV/PI staining. This technique facilitates

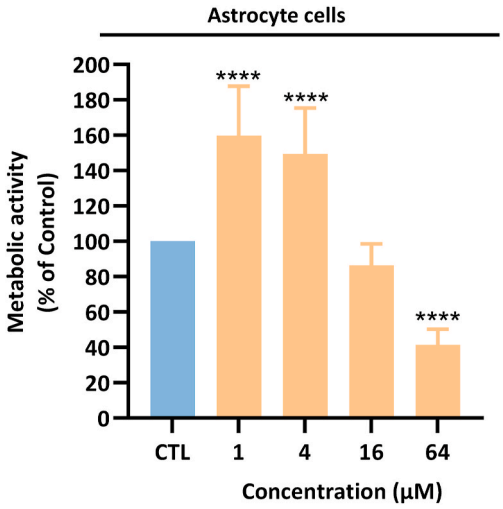

Fig. 4. Impact of Roy on the metabolic activity of non-tumoral cells. Primary astrocyte cells were exposed to Roy's treatment (1, 4, 16, and 64 μM) for 24 h and MTT assay was performed. Metabolic activity was expressed as percentage of control (CTL) (untreated cells). Asterisks (****$p < 0.0001$) represent the values that significantly differ from the control. Data are representative of three independent experiments and are expressed as mean ± SD.

the recognition of live cells from those undergoing apoptosis or necrosis by evaluating membrane permeability and integrity. The experimental setup involved the treatment of all GB cell lines with 16 μM of Roy, a non-toxic concentration for non-tumoral cells (Figs. 3 and 4). After a 48-h treatment period, treated cells were analyzed by flow cytometry (Fig. 5). As anticipated, treatment with Roy led to a notable reduction in the percentage of viable cells compared to untreated control cells (Fig. 5A, B, 5D, and 5E), with exception for H4 cells, for which a significant difference was not observed (Fig. 5C). Concomitant with these findings, we measured a significant increase in the proportion of cells in the early and late stages of apoptosis/necrosis (Fig. 5A, B, 5D, and 5E). Additionally, a higher percentage of cells in early apoptosis was observable in U87, U373, and U118 cells (Fig. 5A, D, and 5E), while an increasing number of cells entered the late stages of apoptosis/necrosis within A172 cells (Fig. 5B).

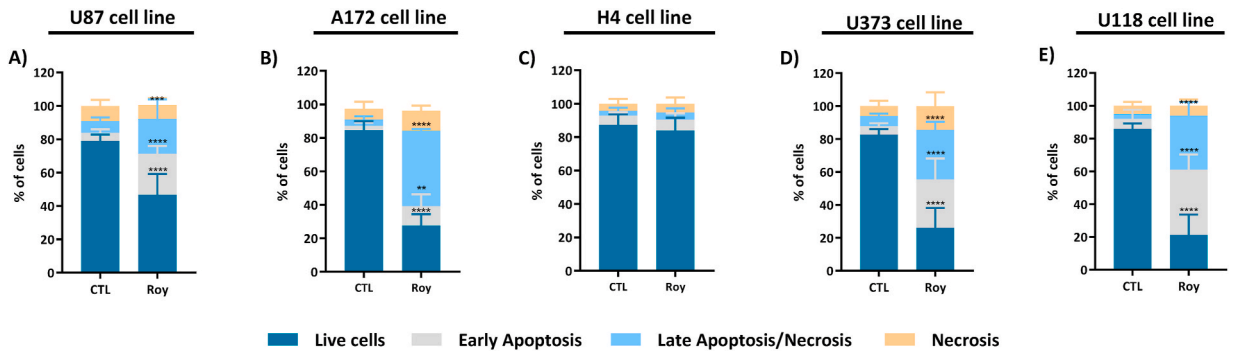

Fig. 5. Cell death profile in U87 **(A)**, A172 **(B)**, H4 **(C)**, U373 **(D)**, and U118 **(E)** cell lines after treatment with Roy. Cells were treated with 16 μM of Roy and further incubated for 48 h. After, cells were co-stained with Annexin V and PI, and the percentage of non-apoptotic cells or cells in apoptosis was determined by flow cytometry. Asterisks (**$p < 0.01$, ***$p < 0.001$, and ****$p < 0.0001$) represent the values that significantly differ from the control group (CTL) (untreated cells). Data are representative of five independent experiments and are expressed as mean ± SD.

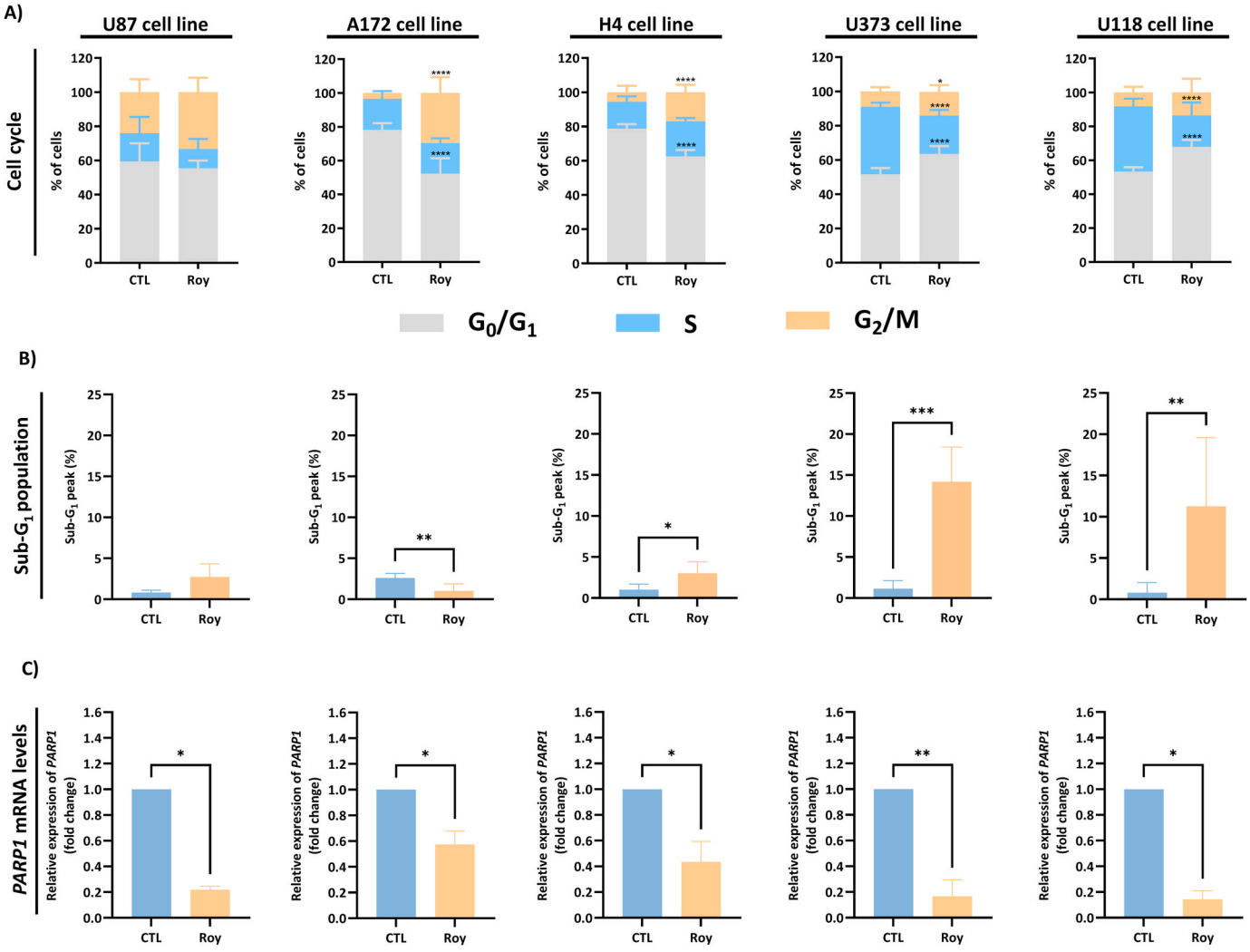

Fig. 6. Effects of Roy on cell cycle progression **(A)**, on DNA fragmentation associated with sub-G_1 peak **(B)**, and *PARP1* mRNA levels **(C)** in U87, A172, H4, U373, and U118 cell lines. Cells were treated with 16 μM of Roy for 48 h. **A)** Cells were stained using a PI/RNase protocol and cell cycle was evaluated by flow cytometry. The proportion of cells in G_0/G_1, S, and G_2/M cell cycle phases was expressed as a percentage of the total cell population. **B)** Sub-G_1 peak associated with DNA fragmentation was assessed using PI/RNase staining protocol. Data was expressed in percentage of cells in Sub-G_1. **C)** Relative expression of *PARP1* mRNA levels was assessed by qRT-PCR and the results normalized to *GAPDH* expression. Asterisks (*$p < 0.05$, **$p < 0.01$, ***$p < 0.001$, and ****$p < 0.0001$) represent values that significantly differ from the control group (CTL) (untreated cells). Data are representative of five independent experiments and are expressed as mean ± SD.

3.3. Roy effect in cell cycle regulation of GB cells

Considering the increase in the population of cells undergoing early and late apoptosis (Fig. 5), as well as the potential cytostatic activity of Roy, we explored the effects of Roy treatment on cell cycle regulation. This analysis was performed by flow cytometry, using a PI/RNase staining protocol (Fig. 6A and B). By quantifying DNA content, we were able to identify a distinct arrest in G_2/M phase in U87, A172, and H4 cells, while such effect was not as evident in U373 and U118 cells, being observed an arrest in G_0/G_1 phase, when comparing to the control condition (untreated cells) (Fig. 6A). Notably, DNA fragmentation was discernible as a sub-G_1 peak upon Roy treatment in U373 and U118 cells (Fig. 6B). In addition, Roy treatment induced a decrease in *PARP1* mRNA levels in all GB cell lines (Fig. 6C), probably indicating an inhibition of DNA repair mechanisms and, subsequently, preventing cells from entering mitosis. Taken together, these results support our observations with AV/PI staining, where we detected a higher percentage of cells undergoing apoptosis (Fig. 5). Interestingly, although treatment of H4 cells with 16 μM Roy had no visible effect on metabolic activity (Fig. 2) and cell death profile (Fig. 5C), an increase in cells in the G_2/M phase and a reduction in *PARP1* mRNA levels is easily visible (Fig. 6A and C).

3.4. Effect of roy on mitochondrial membrane potential of GB cells

Following, we investigated potential effects on mitochondria potentially explaining Roy-triggered cell death, a facet we analyzed using JC-1 staining and flow cytometry (Gonçalves et al., 2013). JC-1, a cationic and lipophilic dye, accumulates within mitochondria, forming red-fluorescent aggregates in healthy cells. Contrarily, in apoptotic cells, the mitochondrial membrane potential collapses, leading to an inability of JC-1 to aggregate inside the mitochondria and resulting in green monomers. This results in JC-1 retaining its monomeric form within the cytosol. Consequently, an increase in the monomer/aggregate (M/A) ratio correlates with a decrease in mitochondrial membrane potential and, by extension, an increase in cells undergoing apoptosis.

Across all GB cell lines, a statistically significant increase in the M/A ratio was noted in conditions treated with Roy when compared to untreated cells (control condition) (Fig. 7). Furthermore, the increase of the M/A ratio was particularly pronounced within GB (Fig. 7A and B) and astrocytoma/GB (Fig. 7D and E) cells following exposure to 16 μM of Roy. Conversely, neuroglioma cells displayed the lowest M/A ratios (Fig. 7C). Nonetheless, a consistent trend was evident in all GB cell lines, with the M/A ratio increasing with Roy treatment (Fig. 7).

3.5. Roy effect on tumor suppressor genes mRNA levels and anti-apoptotic proteins expression in GB cells

In the context of the aforementioned findings, it became evident that Roy can cause GB cell death. With this in mind, we measured the mRNA levels of tumor suppressor genes and oncogenes involved in signaling pathways associated with proliferation and cell death. The transcriptional profiles of *PTEN*, *TP53*, *MDM2*, *BCL2*, and *BCL2L1* were evaluated in GB cells following a 48-h Roy treatment period (Fig. 8). Notably, we observed that Roy's treatment prompted an upregulation of transcripts related to tumor suppressor genes, namely *PTEN* and *TP53* (found to be downregulated in GB cells), in comparison to the control group (untreated cells) (Fig. 8). Moreover, we also observed the downregulation of *MDM2* mRNA expression, a proto-oncogene and negative regulator of p53 expression, was verified upon treatment with Roy, supporting the observed increase of *TP53* mRNA levels (Fig. 8).

Additionally, after treatment with Roy, mRNA levels of the anti-apoptotic genes *BCL2L1* and *BCL2* were found to be decreased (Fig. 8), accompanied by a decrease in Bcl-2 and p21 protein levels (Fig. 9), which may indicate activation of pro-apoptotic mechanisms. Both proteins, Bcl-2 and cytoplasmatic p21, are found to be upregulated in gliomas and are responsible for the inhibition of cell death and progression of cancer.

3.6. Roy effect in caspase levels of GB cells

To evaluate the potential of Roy treatment to induce caspase-mediated cell death, we assessed *CASP9* mRNA levels and quantified activated caspase-3 — a final effector caspase involved in programmed cell death. The outcomes yielded a twofold effect of Roy treatment: all GB cell lines displayed a tendency for the upregulation of *CASP9* mRNA levels (Fig. 10A) and an increase in the proportion of cells expressing activated caspase-3 (Fig. 10B), in comparison with the control group. These findings are aligned with our expectations, given that *CASP9*, the gene encoding the caspase-9 protein, assumes the role of an initiator caspase, orchestrating the activation of caspase-3. This gives substantial credence to the proposition that Roy elicited a programmed cell death executed through apoptosis, underpinned by activation of the caspase cascade.

3.7. Internalization of fluorescently-labeled roy and its effect on the mitochondrial morphology in GB cells

To complement the findings presented within this study, we investigated the uptake of Roy in GB cells and its effect on the mitochondrial morphology using confocal microscopy. We added Roy conjugated with a fluorescent probe (Roy-BODIPY) to GB cells and incubated them with MitoTracker red and Hoechst 33342 to label the mitochondrial network

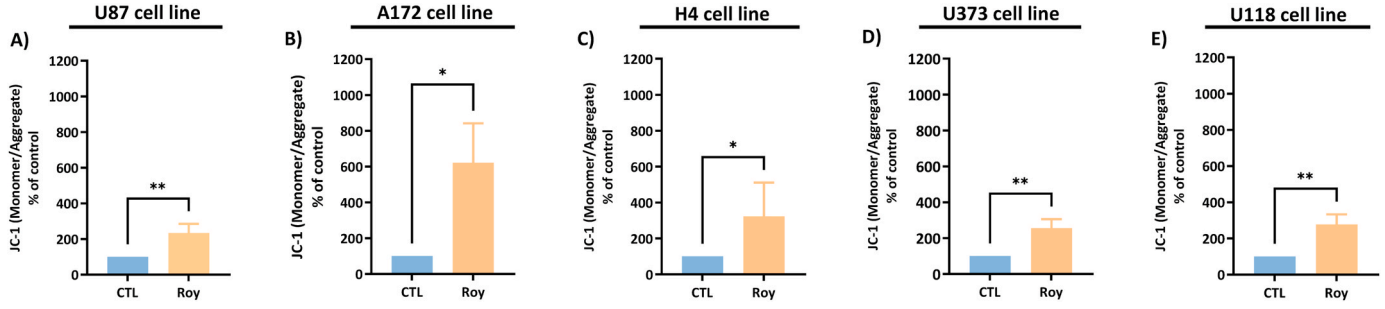

Fig. 7. Analysis of mitochondrial membrane potential ($\Delta\psi_{mit}$) in U87 **(A)**, A172 **(B)**, H4 **(C)**, U373 **(D)**, and U118 **(E)** cell lines. After treatment with 16 μM of Roy for 48 h, cells were incubated with the JC-1 probe and analyzed by flow cytometry. The monomeric or aggregate form of JC-1 probe depends on the mitochondrial membrane potential. An increase in the monomer/aggregate (M/A) ratio indicates a decrease in the mitochondrial polarization. Data are expressed as M/A ratio of JC-1, which was calculated as the fraction of MFI observed for each molecule. Asterisks ($*p < 0.05$ and $**p < 0.01$) represent the values that significantly differ from the control condition (CTL) (untreated cells). Data were presented as mean ± SD and are representative of five independent experiments.

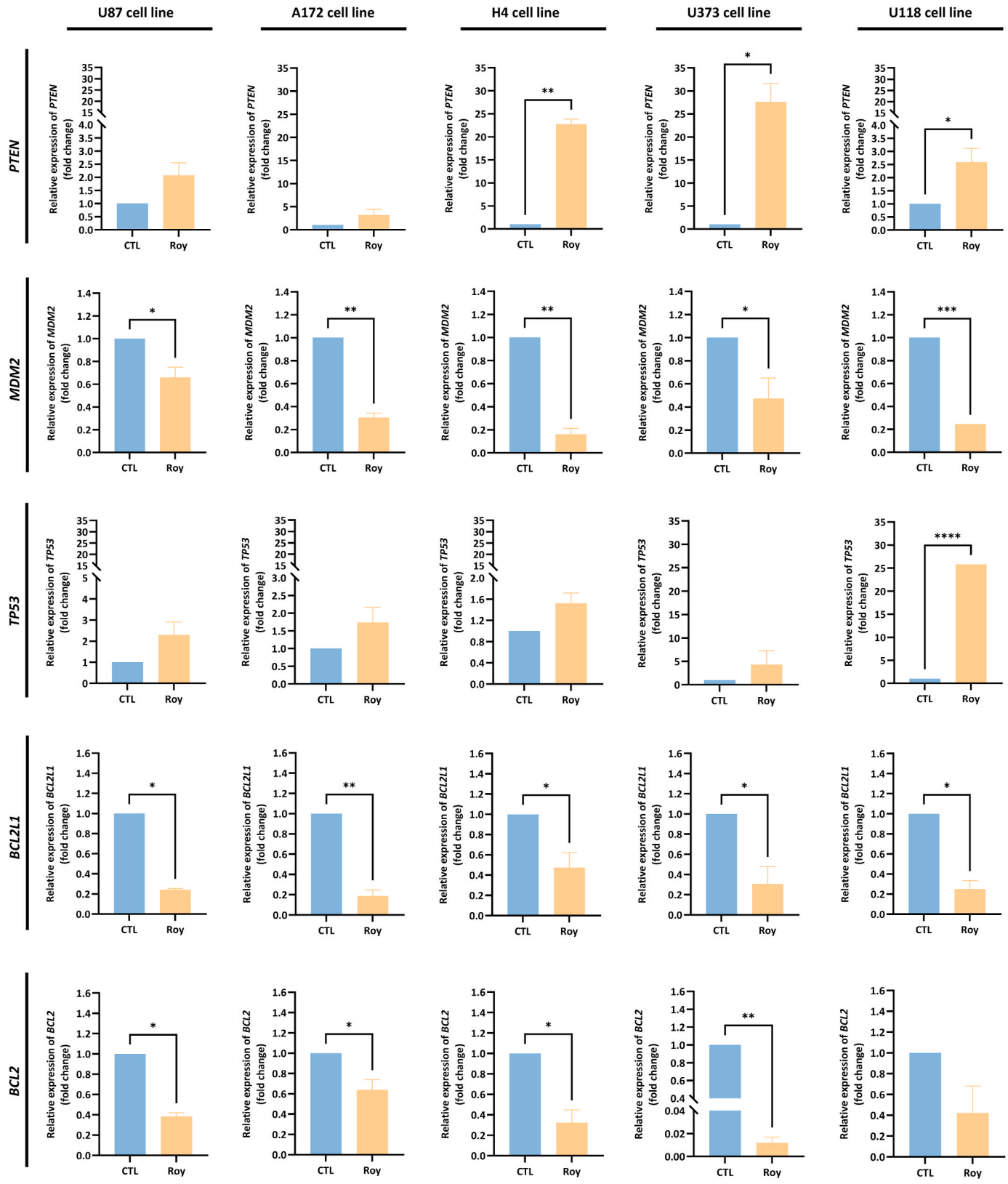

Fig. 8. Assessment of *PTEN*, *MDM2*, *TP53*, *BCL2L1*, and *BCL2* mRNA levels in U87, A172, H4, U373, and U118 cells, after Roy treatment (16 μM) for 48 h. After incubation, the relative expression of *PTEN*, *MDM2*, *TP53*, *BCL2L1*, and *BCL2* was assessed by qRT-PCR, and the results normalized to *GAPDH* expression. Asterisks ($^{*}p < 0.05$ and $^{**}p < 0.01$) represent the values that significantly differ from the control condition (CTL) (untreated cells). Data are presented as mean ± SD and it is representative of five independent experiments.

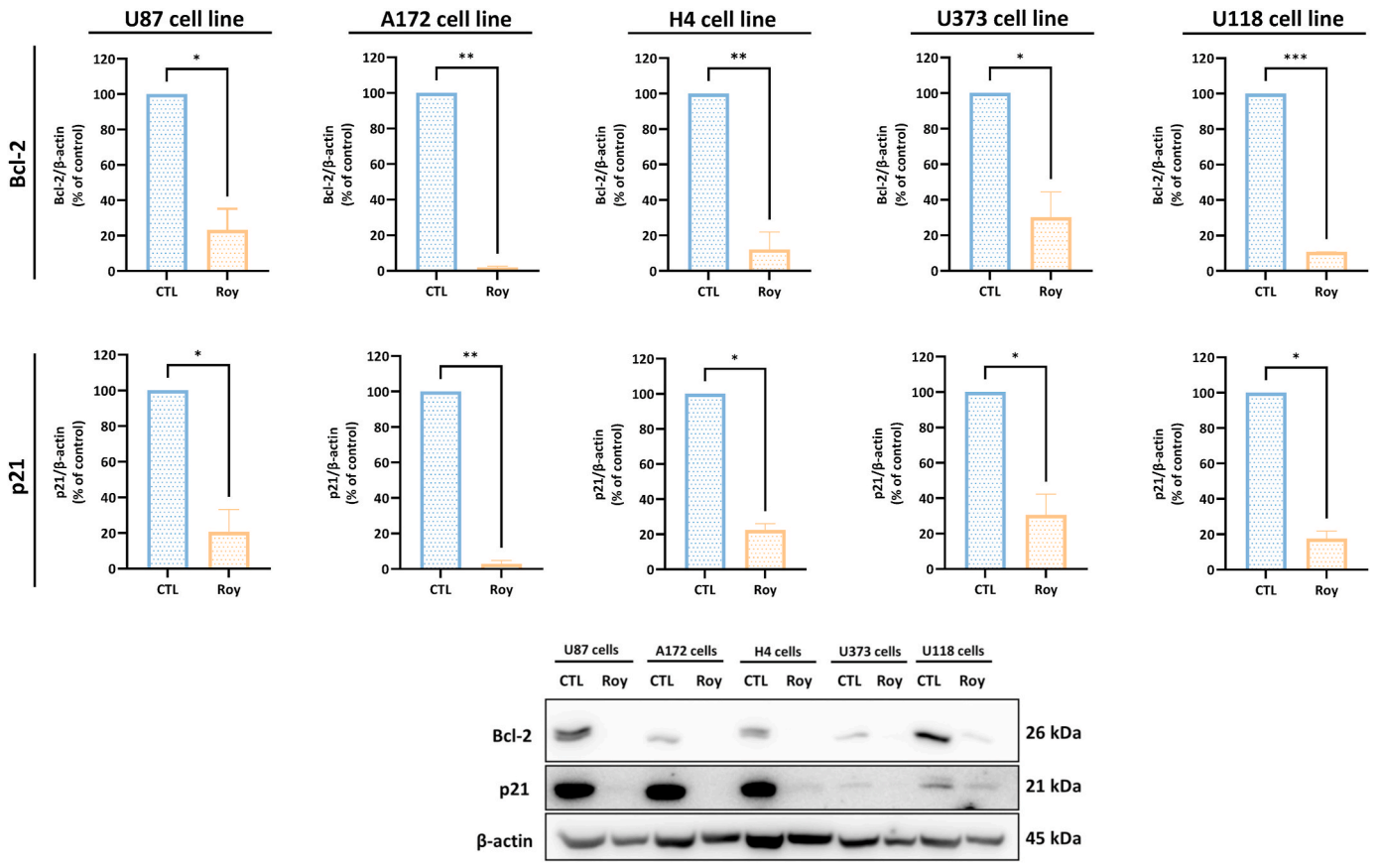

Fig. 9. Impact of Roy in the expression of the anti-apoptotic proteins, Bcl-2 and cytoplasmic p21, in U87, A172, H4, U373 and U118 cells. Representative Western blot result and protein content of Bcl-2, p21, and β-actin (cytosolic marker) in whole-cell homogenates from untreated cells or cells treated with Roy (16 μM) for 48 h. Blots were inverted and contrast-optimized for visualization purposes. Quantification of the bands was performed using the original blots. Quantification of protein levels was normalized to β-actin levels and to the control condition (untreated cells) and representative of three independent assays.

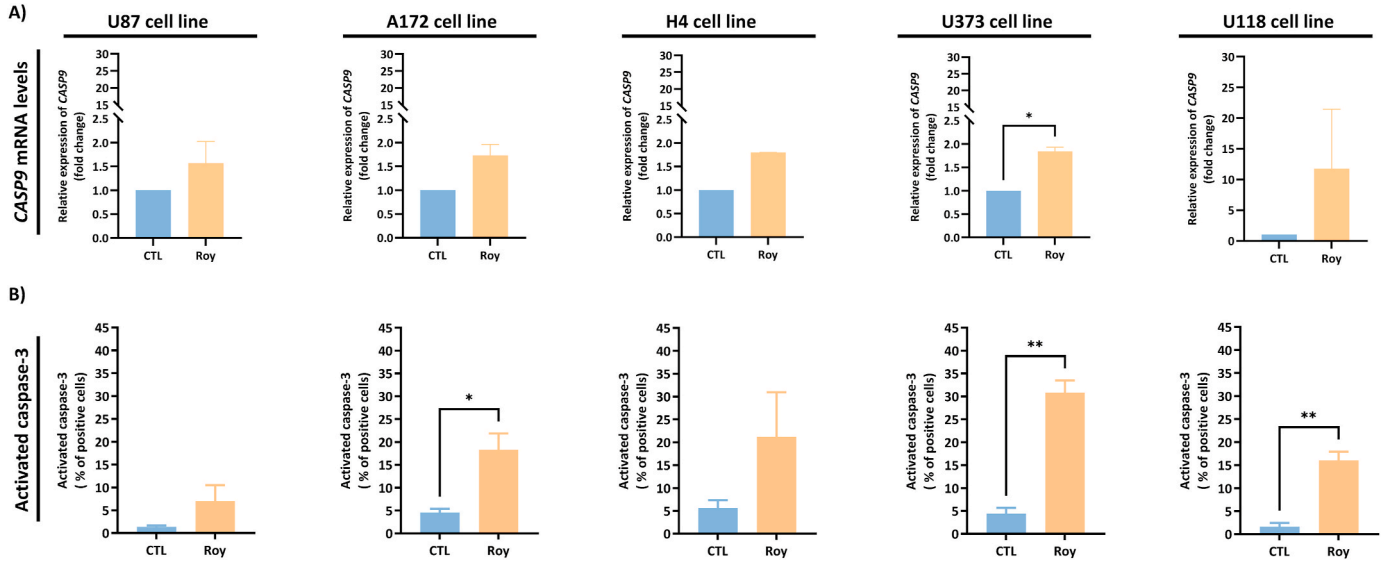

Fig. 10. Analysis of caspase-mediated cell death in U87, A172, H4, U373, and U118 cells after treatment with 16 μM Roy for 48 h. **A)** Relative expression of *CASP9* mRNA levels was assessed by qRT-PCR and the results normalized to *GAPDH* expression. **B)** Activated caspase-3 expression levels as a percentage (%) of positive cells were measured by flow cytometry. Asterisks (*$p < 0.05$ and ***$p < 0.001$) represent the values that significantly differ from the control condition (CTL) (untreated cells). Data are presented as mean ± SD and it is representative of five independent experiments.

and nuclei, respectively, and imaged using confocal microscopy (Fig. 11). Roy exhibited the ability to be internalized by GB, neuroglioma, and astrocytoma/GB cells and be accumulated within the cytoplasm (Fig. 11). Furthermore, a quantitative assessment of mitochondrial morphological traits revealed Roy's capability to induce structural modifications in mitochondria within GB cells, including

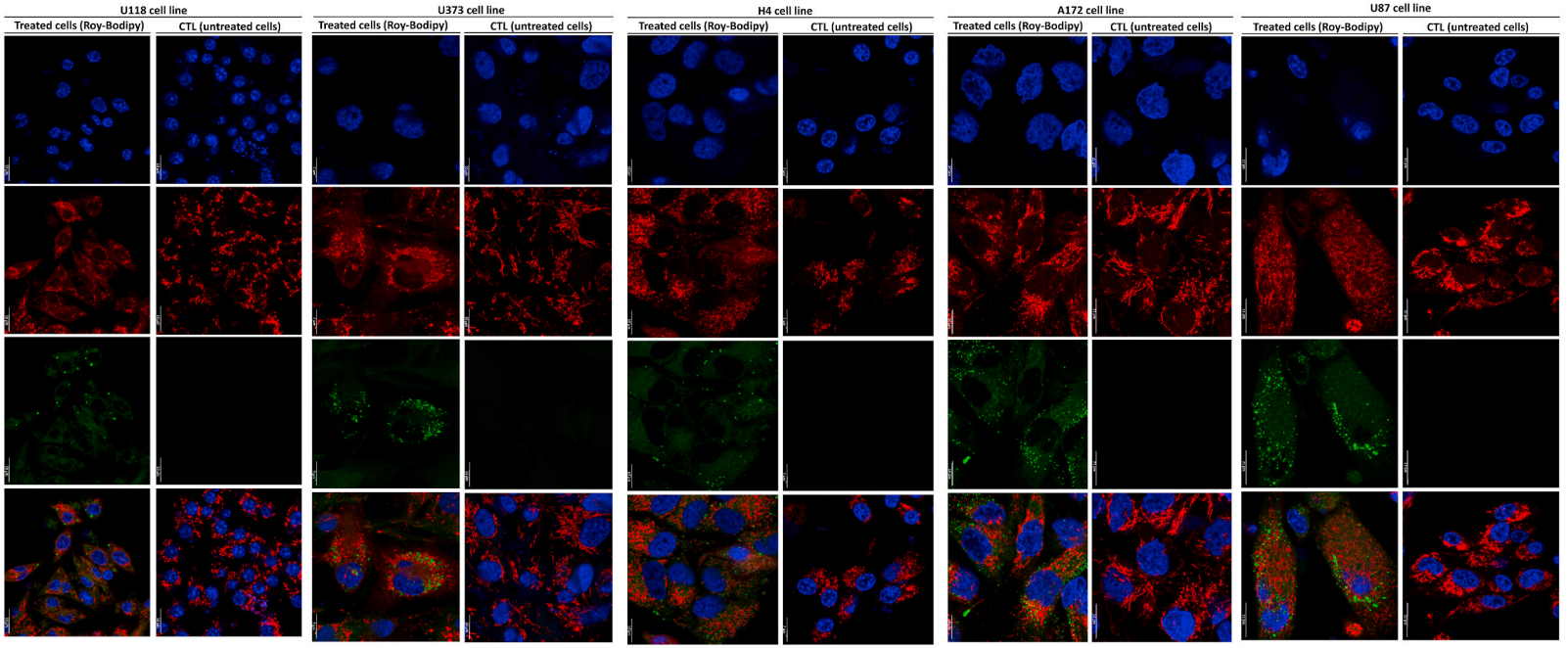

Fig. 11. Cellular uptake of Roy-bodipy in U87, A172, H4, U373, and U118 cells. Cells were treated with 16 μM of Roy for 48 h and further analyzed by confocal microscopy. Representative background-corrected image of GB cells stained with the fluorescent probes MitoTracker red, Hoechst 33342, and BODIPY in untreated cells and cells treated with 16 μM of Roy-BODIPY for 48h. Hoechst 33342, MitoTracker red, and BODIPY fluorescence intensities were color-coded to blue, red, and green, respectively. (For interpretation of the references to color in this figure legend, the reader is referred to the Web version of this article.)

changes in the size, represented by the reduction in mean area and perimeter, as well as alterations in shape, reflected by decreases in FF and AR, metrics assessing mitochondrial elongation and perimeter (Supplementary Fig. S1) (Chaudhry et al., 2019). This analysis suggests that Roy triggers mitochondrial fragmentation in GB cells, consistent with the previously observed decrease in mitochondrial membrane potential (Fig. 7) (Miyazono et al., 2018). However, in U118 cells, Roy appears to have no discernible effect on mitochondrial morphology (Supplementary Fig. S1), despite the significant decrease in mitochondrial membrane potential (Fig. 7E) and an increase in cells undergoing early apoptosis (Figs. 5E and 6B).

This visual validation and quantitative analysis serve as a tangible reinforcement of the observed antitumor impact in GB cells upon exposure to a concentration of 16 μM of Roy.

4. Discussion

The pursuit of effective treatments for cancer has driven the exploration of diverse therapeutic avenues, including the very diverse molecules from natural sources. Natural products are an important reservoir of biologically active molecules with high therapeutic significance, with an important role in the discovery of novel anticancer drugs (Howes, 2018; Naeem et al., 2022; Rodrigues et al., 2016). Their inherent complexity and distinct molecular structures have provided a unique array of therapeutic mechanisms by which they can interfere with cancer cell growth and survival pathways, having an immunomodulatory role (Rayan et al., 2017; Rodrigues et al., 2016). In this context, the conceptualization of innovative treatments grounded in natural lead compounds appears as a plausible approach to address the challenge posed by GB. This grade 4 glioma remains one of the most challenging cancers to treat due to its heterogeneity, aggressive nature, infiltrative growth, and resistance to conventional therapies (Louis et al., 2021; Magalhães et al., 2023). Regarding this, terpenes, a prominent class of secondary metabolites in plants, are an example of natural compounds with enhanced therapeutic potential, including marked antitumor properties, that are worth exploring for designing future therapies for GB (Domínguez-Martín et al., 2023). In addition, terpenes alluring bioactivities have already rendered them noteworthy assets across diverse industries, such as cosmetics and pharmaceuticals (Howes, 2018; Magalhães et al., 2022; Yang et al., 2020).

Thus, during this work, we addressed the potential antitumor activity of Roy, an abietane diterpene, proposing it as a good natural lead compound for tackling GB via novel therapeutic approaches. The chemotherapeutic potential of Roy was evaluated within a panel of five glioma cell lines. This strategy aimed to mimic *in vitro* the heterogeneity exhibited by GB, as these cell lines express distinct molecular signatures associated with the molecular subtypes identified in this tumor (proneural, classical, and mesenchymal), which can manifest *de novo* or evolve from low-grade gliomas (Lane et al., 2019; Magalhães et al., 2023; Verhaak et al., 2010).

Treatment with Roy led to a reduction in the metabolic activity of GB cells, being this effect more pronounced when compared to the standard TMZ treatment (first-line therapy). Across all cell lines, the concentrations of Roy needed to achieve a 50% reduction in cell viability were notably lower than the concentrations of TMZ required to produce similar outcomes. Moreover, lower concentrations of Roy (16 μM) were able to affect the metabolic activity of tumoral cells, without the same impact in non-tumoral cells being observed (HMC3 microglia cell line and primary astrocyte cells). Although, for 64 μM, Roy exhibited a significantly high cytotoxicity in non-tumoral cells, showing a concentration-dependent tumor-specificity. This preliminary analysis underscores the inherent antitumor effect of Roy against GB cells, consistent with the cytotoxic profile observed for this diterpene in previous studies (Domínguez-Martín et al., 2022; Sitarek et al., 2020; Śliwiński et al., 2020), being the potential antitumor mechanism of Roy further explored in this study. As expected, the assessment of cell death revealed that Roy administration induced apoptosis in GB cells, consistent with *in silico* studies predicting that Roy targets genes involved in cancer pathways, particularly those related to apoptotic signaling and programmed cell death (Isca et al., 2024; Merecz-Sadowska et al., 2024). This was further supported by a decrease in mitochondrial membrane potential in GB cells following Roy treatment, a shift that corresponds with the onset of apoptosis (Gonçalves et al., 2013). This effect was particularly significative in U373 and U118 cells, being observed an increase in sub-G_1 phase, which corresponds to DNA fragmentation and is closely linked to heightened apoptotic cells (Plesca et al., 2008). Moreover, a discernible increase in the population of cells within the G_2/M phase was observed for U87, A172, and H4 cells, while, for U373 and U118 cells, was identified an arrest at G_0/G_1 phase. Notably, all cell lines showed a decrease in *PARP1* mRNA levels following Roy treatment, a gene encoding PARP1, a critical protein in DNA damage repair mechanisms. PARP1, reported to be upregulated in cancer including GB, plays a role in enhancing anti-apoptotic mechanisms, leading to resistance against therapeutic agents, which makes this protein a major target for anticancer therapies (Majuelos-Melguizo et al., 2022; Murnyák et al., 2017; Wang et al., 2022). A study by Rao and colleagues, employing both *in silico* and *in vitro* approaches, demonstrated that inhibiting PARP1 in GB enhances sensitivity to TMZ, supporting PARP1 role in GB progression and resistance to treatment. In their research, the authors used a combination treatment of TMZ and narigin, a natural bioflavonoid, to target and reduce PARP1 activity. This approach successfully reversed TMZ resistance, thereby increasing the effectiveness of the treatment (Rao et al., 2021). Therefore, it is plausible that Roy induces DNA damage, activating checkpoint responses regulated by the tumor suppressor pathways of p53 and retinoblastoma protein (pRB). This leads to a cytostatic effect by hindering cell proliferation and enforcing cell cycle arrest at the G_1 and G_2/M phases. This effect likely arises from Roy's ability to inhibit DNA repair mechanisms, targeting *PARP1* gene, preventing the initiation of DNA synthesis, and stopping damaged cells from entering mitosis, ultimately leading to apoptosis (Kastan and Bartek, 2004; Murnyák et al., 2017; Pan et al., 2019; Sitarek et al., 2020).

Moreover, downregulation of the oncogene *MDM2* mRNA levels and upregulation of tumor suppressor genes *PTEN* and *TP53* mRNA levels were observed in GB cells following Roy treatment in comparison to non-treated cells. *PTEN* and *TP53* genes, important biomarkers in GB, are downregulated and mutated in this tumor. These alterations are commonly observed in the mesenchymal subtype, the most aggressive form, but can also occur in other molecular subtypes (Koul, 2008; Ludwig and Kornblum, 2017; Verhaak et al., 2010; Zhang et al., 2018). A recent study showed that the depletion of the tumor suppressor genes *TP53*, *PTEN*, and *NF1* led to the development of GB in 3D human brain organoid cultures, particularly associated with the proneural subtype, supporting the crucial role of these genes in the tumorigenesis process (Singh et al., 2023). *PTEN,* a negative regulator of the phosphatidylinositol 3-kinase (PI3K)/protein kinase B (Akt) signaling cascade, that is upregulated in the context of GB, and *TP53*, the encoding gene for the p53 protein—a pivotal transcriptional regulator recognized as the "guardian of the genome"—acted as sentinels responding to stress signals, preventing DNA damage while inducing apoptosis and arresting cell cycle (Abraham and O'Neill, 2014; Koul, 2008). Therefore, this could suggest suppression of the PI3K/Akt signaling pathway through heightened *PTEN* mRNA levels, leading to the inhibition of MDM2 expression and activation of p53 following Roy treatment (Pearson and Regad, 2017). A study by Wang and colleagues also underscores the potential of targeting *PTEN* and *TP53*-related signaling pathways. They demonstrated that using the natural compound curcumin to induce downregulation of the Akt pathway resulted in overexpression of PTEN and p53. This, in turn, inhibited proliferation and reduced tumor size in both cell and animal models of GB (Wang et al., 2020). Additionally, downregulation of the anti-apoptotic genes *BCL2L1* and *BCL2* mRNA levels and reduction of Bcl-2 and cytoplasmic p21 protein levels in all GB

cells was also observed following Roy treatment. *BCL2L1* is the gene encoding the Bcl-xl protein, which together with Bcl-2 belongs to the Bcl-2 protein family, which is renowned for its involvement in regulating apoptosis, and its dysregulation can have profound implications for cancer development, progression, and response to therapy (Warren et al., 2019; Weiler et al., 2006). Bcl-2, an anti-apoptotic protein that functions to prevent cells from undergoing apoptosis, is overexpressed in gliomas, although, a decrease in its expression was observed following Roy treatment (Warren et al., 2019). This finding supports the capability of this compound to induce apoptosis in GB cells by targeting apoptotic signaling pathways. Furthermore, overexpression of cytoplasmatic p21, which has been linked to promoting cell survival and resistance to apoptosis in cancer, including glioma, was inhibited after Roy treatment. Despite the oncogenic role of p21 (cytoplasmic p21) in cancer is still an active area of research, it is reported that interaction between cytoplasmic p21 and Bcl-2 may counteract the apoptotic signals initiated by pro-apoptotic factors. This interaction can lead to the suppression of apoptotic pathways and enhance cancer cell survival (Abbas and Dutta, 2009; Shamloo and Usluer, 2019). Herein, upon subjecting GB cells to a lower concentration of Roy, we observed an upregulation of tumor suppressor genes mRNA levels and a decrease in the expression of anti-apoptotic proteins, triggering cell cycle arrest and apoptosis in treated cells. These findings were corroborated by the expression of activated caspase-3, an effector caspase, which was accompanied by upregulation of *CASP9* mRNA levels (encodes caspase-9, an initiator caspase). Caspase-3 is a pivotal protein involved in apoptosis, the programmed cell death that maintains tissue homeostasis by eliminating damaged, unnecessary, or potentially harmful cells (Elmore, 2007; Yadav et al., 2021). Hence, the induction of activated caspase-3 expression through Roy treatment triggered the anticipated apoptosis in GB cells potentially by targeting apoptotic signaling pathways and Bcl-2 family. Bcl-2 family proteins play a central role in regulating apoptosis, and oncogenesis is often linked to their abnormal expression. Bcl-2 and Bcl-xL proteins, known to be overexpressed in cancer, inhibit apoptosis by preventing the release of cytochrome C and the activity of caspases-9, -3, -6, and -7. This inhibition promotes tumor growth and survival, leading to the malignant transformation of cells (Qian et al., 2022). Therefore, suppressing Bcl-2 expression could lower the levels of anti-apoptotic/pro-survival proteins and elevate caspase-3 levels. This, in turn, targets PARP, disrupts DNA repair mechanisms, and ultimately induces apoptosis (Hwang et al., 2019). This underlines that the antitumor mechanism of Roy operates via the initiation of caspase-mediated apoptosis.

Overall, during this work, we delved into the inherent antitumor efficacy of Roy in various human glioma cell lines. In a broad sense, this natural compound affected the mitochondrial network and triggered caspase-mediated apoptosis across all cells. However, we observed distinct mechanisms at play when it came to cell cycle regulation with Roy treatment. For GB and neuroglioma cells, it caused cell cycle arrest in the G_2/M phase, while for astrocytoma/GB cells, it led to arrest in the G_0/G_1 phase. The variation observed among these cell lines may be linked to their distinct molecular signatures associated with GB subtypes (Proneural - U373 and U118 cells; Classical – A172 and H4 cells; and Mesenchymal – U87 cells). U373 and U118 cells, in particular, exhibit a mitotic profile associated with a better response to therapy, likely due to the methylation of the *MGMT* promoter gene, a key mechanism of drug resistance in many cancers (Anan et al., 2024; Brandt et al., 2023; Dunn et al., 2009). Moreover, cell cycle arrest in GB cells following Roy treatment seems to occur because this compound targets the p53 pathway, leading to cell cycle arrest, impaired replication of damaged DNA, and subsequent apoptosis. Additionally, the antitumor effect of Roy was confirmed by the effective internalization of this natural lead compound by GB cells, as evidenced by confocal microscopy. To be noted, Roy induced structural changes in mitochondria within GB cells, thereby triggering mitochondrial fragmentation (tubular to globular shape) and affecting the mitochondrial network. This aligns with the observed decrease of the mitochondrial membrane potential and increase of cell death following treatment with Roy, thus confirming our expectations. However, these structural changes were not observed in U118 cells, despite a notable decrease in mitochondrial membrane potential accompanied with a substantial increase of cells in apoptosis, following treatment. The outcomes of this study underline the robust antitumor impact of Roy on GB cells, channeling apoptosis mediated by activation of the caspase cascade. This modulation likely entails cell cycle arrest, mitochondrial fragmentation, upregulation of tumor suppressor genes, and inhibition of anti-apoptotic proteins.

It is important to acknowledge that conducting a complete *in vitro* study could be a limitation and potential bias of this work. Sampling bias and selection for a high proliferative behavior of cell lines *in vitro* may have some impact on the representation of cancer cell models (Noorbakhsh et al., 2021). Additionally, measures to reduce cross-contamination and acquire cell lines from known repositories to avoid misidentification and ensure authentication are essential. To address these issues, we used a panel of human glioma cell lines obtained from a well-recognized company to capture the heterogeneity of GB, a hallmark of this tumor type, and to be more representative of the population of interest. This approach helps mitigate the challenge of establishing primary cultures from patient samples, which are only obtainable during brain surgery. Throughout this study, we identified other potential biases (*e.g.*, the researcher's bias that, unconsciously, can lead them to a misinterpretation of data due to prior knowledge and results expectation) and addressed them by maintaining standardized culture conditions and protocols, keeping detailed records of cell line, passage number, and experimental conditions, conducting experiments in multiple cell lines and replicating studies to ensure robustness, sharing data and methods openly to facilitate reproducibility, and performing a rigorous peer review of the experimental design, data interpretation and analysis.

To sum up, this study successfully identified Roy as a novel and promising natural lead compound with potent antitumoral properties against GB cell models. Through a single administration at a low concentration, Roy demonstrated a stronger therapeutic effect compared to the standard chemotherapeutic drug. Despite modest improvements in the overall survival of GB patients, treatment success has largely remained unchanged over the past few decades, highlighting the importance of discovering new and effective anticancer molecules. Consequently, as a follow-up to this study and for future translational research, it is crucial to evaluate the effects of Roy in an animal model of GB. Furthermore, incorporating Roy into innovative site-specific pharmaceutical formulations could lead to more effective therapies against this devastating and incurable tumor while reducing off-target risks. Therefore, for further studies, it is essential to investigate the pharmacokinetics, biodistribution, and administration methodology of Roy-loaded formulations in vivo and in pre-clinical models to ensure their efficacy. Additionally, studying the physicochemical properties of these formulations and ensuring their reproducibility and stability over time is critical for efficient scale-up and quality control of the final product. In fact, the development of pharmaceutical formulations incorporating natural lead compounds or their derivatives to treat different types of tumors is already under investigation and evaluation in clinical trials (e.g., NCT05768919; NCT01994031; NCT04796948; NCT06481553; NCT02631733).

Thus, we hope this work serves as a foundation for future research, contributing to alleviating the suffering of patients and their loved ones by surpassing the limitations of conventional treatments.

5. Ethical considerations for future translation of this study

For further studies and future clinical translation, it is crucial to consider ethics and approval processes for animal experimentation and the use of human samples, as these represent the next logical steps. Regarding studies involving this tumor, the GB-induced xenograft

mouse model is the most widely used and well-established model. Rodent models are vital for biomedical research advancement due to their physiological similarity to humans, easy accessibility, and relatively straightforward ethical approval processes compared to human trials (Domínguez-Oliva et al., 2023). When using animal models, researchers must adopt ethical standards that ensure proper treatment and human care of the animals. This approach not only avoids unnecessary suffering but also ensures the best scientific research outcomes and reproducibility, a hallmark of scientific research and a significant issue in many studies. The principle of the 4Rs should be employed: 1) Reduction: Use the minimum number of animal models required to obtain reliable data; 2) Refinement: Reduce the risky effects of experiments by lowering pain; 3) Replacement: Use alternative models, such as *in silico* and *in vitro* approaches, whenever possible. These approaches should always be considered the primary method for conducting a more in-depth and comprehensive study, as we intended to do with this work, with animal studies serving as the final strategy to validate findings; and 4) Responsibility: Prioritize promoting animal welfare (Kiani et al., 2022). In addition to animal models, the use of human brain tissues isolated from GB patients should also be considered. This approach helps address the limitations of cell lines and validates *in vitro* results. Ensuring ethical standards and procedures approved by a recognized Research Ethics Review Committee is essential. This includes implementing an informed consent process and a data protection system (Clarke et al., 2001). Following these procedures and validating our expected outcomes in these models, a translational approach from bench to bedside should be employed for novel therapy. For human trials, it is essential to perform a risk-benefit analysis, provide justification for the research, secure informed consent and confirm its validity, and identify and address any conflicts of interest. These factors are vital for maintaining ethical standards in human research (Koonrungsesomboon et al., 2016).

6. Conclusion

The findings from this study strongly demonstrate that the concentration of Roy required to achieve a 50% reduction in cell viability in GB cells was significantly lower than the concentration needed by TMZ, the first-line treatment, to produce a similar effect. Roy treatment not only hindered genes associated with DNA repair but also triggered caspase-mediated apoptosis. Additionally, Roy suppresses the expression of anti-apoptotic proteins, promoting cell death.

In resume, our research identifies a promising therapeutic approach for treating malignant glioma. It offers a hopeful avenue to overcome the limitations linked to conventional treatments. This underlines the potential of Roy as a prospective natural lead candidate to integrate future therapies for GB. Further studies will be addressed to understand the potential of Roy effect in an animal model of GB.

CRediT authorship contribution statement

Mariana Magalhães: Writing – review & editing, Writing – original draft, Methodology, Investigation, Formal analysis, Conceptualization. **Eva María Domínguez-Martín:** Methodology. **Joana Jorge:** Methodology. **Ana Cristina Gonçalves:** Writing – review & editing, Methodology. **Francesca Massenzio:** Methodology. **Renato Spigarelli:** Methodology. **Teresa Ribeiro-Rodrigues:** Methodology. **Steve Catarino:** Writing – review & editing, Methodology. **Henrique Girão:** Writing – review & editing, Resources. **Barbara Monti:** Writing – review & editing, Resources. **Enzo Spisni:** Writing – review & editing, Resources. **Lino Ferreira:** Writing – review & editing, Resources. **Paulo J. Oliveira:** Writing – review & editing, Resources. **Thomas Efferth:** Writing – review & editing, Supervision, Conceptualization. **Patrícia Rijo:** Writing – review & editing, Resources. **Célia Cabral:** Writing – review & editing, Supervision, Resources, Funding acquisition, Conceptualization.

Declaration of competing interest

The authors declare that they have no known competing financial interests or personal relationships that could have appeared to influence the work reported in this paper.

Data availability

Data will be made available on request.

Acknowledgments

We would like to thank the support provided by Foundation for Science and Technology (FCT, Portugal), through the following projects: UIDB/04539/2020, UIDP/04539/2020, and LA/P/0058/2020 (CIBB) Strategic Projects. M.M. is supported by a Foundation for Science and Technology (FCT) PhD grant (Reference: SFRH/BD/146441/2019). J.J. is supported by a Foundation for Science and Technology (FCT) PhD grant (Reference: SFRH/BD/145531/2019). These PhD grants are financed by national budget and co-financed through the European Social Fund (ESF) and the Regional Operational Por_Centro. E.M.D-M gratefully acknowledges being the recipient of a predoctoral FPU-UAH 2019 fellowship from University of Alcalá de Henares. The authors would like to thank the support of iLAB – Microscopy and Bioimaging Lab a facility of Faculty of Medicine of University of Coimbra, and member of the national infrastructure PPBI-Portuguese Platform of BioImaging (POCI-01-0145-FEDER-022122) and supported by FSE CENTRO-04-3559-FSE-000142.

Appendix A. Supplementary data

Supplementary data to this article can be found online at https://doi.org/10.1016/j.jep.2024.118689.

References

Abbas, T., Dutta, A., 2009. p21 in cancer: intricate networks and multiple activities. Nat. Rev. Cancer 9, 400–414. https://doi.org/10.1038/nrc2657.

Abraham, A.G., O'Neill, E., 2014. PI3K/Akt-mediated regulation of p53 in cancer. Biochem. Soc. Trans. 42, 798–803. https://doi.org/10.1042/BST20140070.

Alves, R., Gonçalves, A.C., Jorge, J., Alves, J., Alves da Silva, A., Freitas-Tavares, P., Nascimento Costa, J.M., Almeida, A.M., Sarmento-Ribeiro, A.B., 2019. Everolimus in combination with Imatinib overcomes resistance in Chronic myeloid leukaemia. Med. Oncol. 36, 30. https://doi.org/10.1007/s12032-019-1253-5.

Anan, M., Del Maestro, R.F., Hata, N., Fujiki, M., 2024. O-methylguanine methyltransferase promoter methylation status of glioblastoma cell line clonal population. Neuropathology 44, 41–46. https://doi.org/10.1111/neup.12931.

Angom, R.S., Nakka, N.M., Bhattacharya, S., 2023. Advances in glioblastoma therapy: an update on current approaches. Brain Sci. 13 https://doi.org/10.3390/brainsci13111536.

Bangay, G., Brauning, F.Z., Rosatella, A., Díaz-Lanza, A.M., Domínguez-Martín, E.M., Goncalves, B., Hussein, A.A., Efferth, T., Rijo, P., 2024. Anticancer diterpenes of African natural products: mechanistic pathways and preclinical developments. Phytomedicine 129, 155634. https://doi.org/10.1016/j.phymed.2024.155634.

Brandt, B., Németh, M., Berta, G., Szünstein, M., Heffer, M., Rauch, T.A., Pap, M., 2023. A promising way to overcome temozolomide resistance through inhibition of protein neddylation in glioblastoma cell lines. Int. J. Mol. Sci. 24 https://doi.org/10.3390/ijms24097929.

Chaudhry, A., Shi, R., Luciani, D.S., 2019. A pipeline for multidimensional confocal analysis of mitochondrial morphology, function, and dynamics in pancreatic β-cells. Am. J. Physiol. Metab 318, E87–E101. https://doi.org/10.1152/ajpendo.00457.2019.

Chien, C.-H., Hsueh, W.-T., Chuang, J.-Y., Chang, K.-Y., 2021. Dissecting the mechanism of temozolomide resistance and its association with the regulatory roles of intracellular reactive oxygen species in glioblastoma. J. Biomed. Sci. 28, 18. https://doi.org/10.1186/s12929-021-00717-7.

Clarke, A., English, V., Harris, H., Wells, F., 2001. Ethical considerations. Int. J. Pharmaceut. Med. 15, 89–94. https://doi.org/10.1097/00124363-200104000-00012.

Clinic, M., 2024. https://www.mayoclinic.org/drugs-supplements/temozolomide-oral-route/proper-use/drg-20066228 [WWW Document].

Domínguez-Martín, E.M., Magalhães, M., Díaz-Lanza, A.M., Marques, M.P., Princiotto, S., Gómez, A.M., Efferth, T., Cabral, C., Rijo, P., 2022. Phytochemical study and antiglioblastoma activity assessment of plectranthus hadiensis (forssk.) Schweinf. Ex

sprenger var. hadiensis stems. Molecules 27. https://doi.org/10.3390/molecules27123813.
Domínguez-Martín, E.M., Magalhães, M., Efferth, T., Díaz-Lanza, A.M., Cabral, C., Rijo, P., 2023. Chapter 12 - terpenes: A hope for glioblastoma patients. In: Vitorino, C., Balaña, C., Cabral, C.B. (Eds.), New Insights into Glioblastoma: Diagnosis, Therapeutics and Theranostics. Academic Press, pp. 227–269. https://doi.org/10.1016/B978-0-323-99873-4.00014-1.
Domínguez-Oliva, A., Hernández-Ávalos, I., Martínez-Burnes, J., Olmos-Hernández, A., Verduzco-Mendoza, A., Mota-Rojas, D., 2023. The importance of animal models in biomedical research: current insights and applications. Animals 13. https://doi.org/10.3390/ani13071223.
Dunn, J., Baborie, A., Alam, F., Joyce, K., Moxham, M., Sibson, R., Crooks, D., Husband, D., Shenoy, A., Brodbelt, A., Wong, H., Liloglou, T., Haylock, B., Walker, C., 2009. Extent of MGMT promoter methylation correlates with outcome in glioblastomas given temozolomide and radiotherapy. Br. J. Cancer 101, 124–131. https://doi.org/10.1038/sj.bjc.6605127.
Elmore, S., 2007. Apoptosis: a Review of programmed cell death. Toxicol. Pathol. 35, 495–516. https://doi.org/10.1080/01926230701320337.
Gonçalves, A.C., Alves, V., Silva, T., Carvalho, C., Oliveira, C.R. de, Sarmento-Ribeiro, A. B., 2013. Oxidative stress mediates apoptotic effects of ascorbate and dehydroascorbate in human Myelodysplasia cells in vitro. Toxicol. Vitro 27, 1542–1549. https://doi.org/10.1016/j.tiv.2013.03.009.
Hazaymeh, M., Löber-Handwerker, R., Döring, K., Abboud, T., Mielke, D., Rohde, V., Malinova, V., 2022. Prognostic differences and implications on treatment strategies between butterfly glioblastoma and glioblastoma with unilateral corpus callosum infiltration. Sci. Rep. 12, 19208 https://doi.org/10.1038/s41598-022-23794-6.
Howes, M.J.R., 2018. The evolution of anticancer drug discovery from plants. Lancet Oncol. 19, 293–294. https://doi.org/10.1016/S1470-2045(18)30136-0.
Hwang, J.Y., Park, J.H., Kim, M.J., Kim, W.J., Ha, K.-T., Choi, B.T., Lee, S.-Y., Shin, H.K., 2019. Isolinderalactone regulates the BCL-2/caspase-3/PARP pathway and suppresses tumor growth in a human glioblastoma multiforme xenograft mouse model. Cancer Lett. 443, 25–33. https://doi.org/10.1016/j.canlet.2018.11.027.
Isca, V.M.S., Sitarek, P., Merecz-Sadowska, A., Małecka, M., Owczarek, M., Wieczfińska, J., Zajdel, R., Nowak, P., Rijo, P., Kowalczyk, T., 2024. Anticancer effects of abietane diterpene 7α-Acetoxy-6β-hydroxyroyleanone from plectranthus grandidentatus and its semi-synthetic analogs: an in silico computational approach. Molecules 29. https://doi.org/10.3390/molecules29081807.
Kastan, M.B., Bartek, J., 2004. Cell-cycle checkpoints and cancer. Nature 432, 316–323. https://doi.org/10.1038/nature03097.
Kiani, A.K., Pheby, D., Henehan, G., Brown, R., Sieving, P., Sykora, P., Marks, R., Falsini, B., Capodicasa, N., Miertus, S., Lorusso, L., Dondossola, D., Tartaglia, G.M., Ergoren, M.C., Dundar, M., Michelini, S., Malacarne, D., Bonetti, G., Dautaj, A., Donato, K., Medori, M.C., Beccari, T., Samaja, M., Connelly, S.T., Martin, D., Morresi, A., Bacu, A., Herbst, K.L., Kapustin, M., Stuppia, L., Lumer, L., Farronato, G., Bertelli, M., 2022. Ethical considerations regarding animal experimentation. J. Prev. Med. Hyg. 63, E255–E266. https://doi.org/10.15167/2421-4248/jpmh2022.63.2S3.2768.
Koonrungsesomboon, N., Laothavorn, J., Karbwang, J., 2016. Ethical considerations and challenges in first-in-human research. Transl. Res. 177, 6–18. https://doi.org/10.1016/j.trsl.2016.05.006.
Koul, D., 2008. PTEN signaling pathways in glioblastoma. Cancer Biol. Ther. 7, 1321–1325. https://doi.org/10.4161/cbt.7.9.6954.
Kow, C.Y., Kim, B.J.H., Park, T.I.-H., Chen, J.C.C., Vong, C.K., Kim, J.Y., Shim, V., Dragunow, M., Heppner, P., 2020. Extent of resection affects prognosis for patients with glioblastoma in non-eloquent regions. J. Clin. Neurosci. 80, 242–249. https://doi.org/10.1016/j.jocn.2020.08.023.
Lane, R., Simon, T., Vintu, M., Solkin, B., Koch, B., Stewart, N., Benstead-Hume, G., Pearl, F.M.G., Critchley, G., Stebbing, J., Giamas, G., 2019. Cell-derived extracellular vesicles can be used as a biomarker reservoir for glioblastoma tumor subtyping. Commun. Biol. 2, 315. https://doi.org/10.1038/s42003-019-0560-x.
Louis, D.N., Perry, A., Wesseling, P., Brat, D.J., Cree, I.A., Figarella-Branger, D., Hawkins, C., Ng, H.K., Pfister, S.M., Reifenberger, G., Soffietti, R., Von Deimling, A., Ellison, D.W., 2021. The 2021 WHO classification of tumors of the central nervous system: a summary. Neuro Oncol. 23, 1231–1251. https://doi.org/10.1093/neuonc/noab106.
Ludwig, K., Kornblum, H.I., 2017. Molecular markers in glioma. J. Neuro Oncol. 134, 505–512. https://doi.org/10.1007/s11060-017-2379-y.
Magalhães, M., Cabral, C., Costa, B.M., Manadas, B., 2023. Chapter 5 - secretome analysis of patient-derived glioblastoma cells for potential biomarker identification. In: Vitorino, C., Balaña, C., Cabral, C. (Eds.), New Insights into Glioblastoma: Diagnosis, Therapeutics and Theranostics. Academic Press, pp. 81–97. https://doi.org/10.1016/B978-0-323-99873-4.00015-3.
Magalhães, M., Domínguez-Martín, E.M., Jorge, J., Gonçalves, A.C., Díaz-Lanza, A.M., Manadas, B., Efferth, T., Rijo, P., Cabral, C., 2022. Parvifloron D-based potential therapy for glioblastoma: inducing apoptosis via the mitochondria dependent pathway. Front. Pharmacol. 13, 1–12. https://doi.org/10.3389/fphar.2022.1006832.
Magalhães, M., Farinha, D., de Lima, M.C.P., Faneca, H., 2014. Increased gene delivery efficiency and specificity of a lipid-based nanosystem incorporating a glycolipid. Int. J. Nanomed. 9, 4979–4989. https://doi.org/10.2147/IJN.S69822.
Majuelos-Melguizo, J., Rodríguez-Vargas, J.M., Martínez-López, N., Delgado-Bellido, D., García-Díaz, Á., Yuste, V.J., García-Macía, M., López, L.M., Singh, R., Oliver, F.J., 2022. Glioblastoma cells counteract PARP inhibition through pro-survival induction of lipid droplets synthesis and utilization. Cancers 14. https://doi.org/10.3390/cancers14030726.
Massenzio, F., Peña-altamira, E., Petralla, S., Virgili, M., Zuccheri, G., Miti, A., Polazzi, E., Mengoni, I., Piffaretti, D., Monti, B., 2018. Microglial overexpression of fALS-linked mutant SOD1 induces SOD1 processing impairment , activation and neurotoxicity and is counteracted by the autophagy inducer trehalose. BBA - Mol. Basis Dis. 1864, 3771–3785. https://doi.org/10.1016/j.bbadis.2018.10.013.
Merecz-Sadowska, A., Isca, V.M.S., Sitarek, P., Kowalczyk, T., Małecka, M., Zajdel, K., Zielińska-Bliźniewska, H., Jęcek, M., Rijo, P., Zajdel, R., 2024. Exploring the anticancer potential of semisynthetic derivatives of 7α-Acetoxy-6β-hydroxyroyleanone from plectranthus sp.: an in silico approach. Int. J. Mol. Sci. 25 https://doi.org/10.3390/ijms25084529.
Miyazono, Y., Hirashima, S., Ishihara, N., Kusukawa, J., Nakamura, K., Ohta, K., 2018. Uncoupled mitochondria quickly shorten along their long axis to form indented spheroids, instead of rings, in a fission-independent manner. Sci. Rep. 8, 350. https://doi.org/10.1038/s41598-017-18582-6.
Murnyák, B., Kouhsari, M.C., Hershkovitch, R., Kálmán, B., Marko-Varga, G., Klekner, Á., Hortobágyi, T., 2017. PARP1 expression and its correlation with survival is tumour molecular subtype dependent in glioblastoma. Oncotarget 8. https://doi.org/10.18632/oncotarget.18013.
Naeem, A., Hu, P., Yang, M., Zhang, J., Liu, Y., Zhu, W., Zheng, Q., 2022. Natural products as anticancer agents: current status and future perspectives. Molecules 27. https://doi.org/10.3390/molecules27238367.
Noorbakhsh, J., Vazquez, F., McFarland, J.M., 2021. Bridging the gap between cancer cell line models and tumours using gene expression data. Br. J. Cancer 125, 311–312. https://doi.org/10.1038/s41416-021-01359-0.
Ntungwe, E., Domínguez-Martín, E.M., Teodósio, C., Teixidó-Trujillo, S., Armas Capote, N., Saraiva, L., Díaz-Lanza, A.M., Duarte, N., Rijo, P., 2021. Preliminary biological activity screening of Plectranthus spp. extracts for the search of anticancer lead molecules. Pharmaceuticals 14. https://doi.org/10.3390/ph14050402.
Ortiz, R., Perazzoli, G., Cabeza, L., Jiménez-Luna, C., Luque, R., Prados, J., Melguizo, C., 2021. Temozolomide: an updated overview of resistance mechanisms, nanotechnology advances and clinical applications. Curr. Neuropharmacol. 19, 513–537. https://doi.org/10.2174/1570159X18666200626204005.
Pan, Z., Zhang, X., Yu, P., Chen, X., Lu, P., Li, M., Liu, X., Li, Z., Wei, F., Wang, K., Zheng, Q., Li, D., 2019. Cinobufagin induces cell cycle arrest at the G2/M phase and promotes apoptosis in malignant melanoma cells. Front. Oncol. 9 https://doi.org/10.3389/fonc.2019.00853.
Pearson, J.R.D., Regad, T., 2017. Targeting cellular pathways in glioblastoma multiforme. Signal Transduct. Targeted Ther. 2, 17040 https://doi.org/10.1038/sigtrans.2017.40.
Plesca, D., Mazumder, S., Almasan, A.B., 2008. DNA damage response and apoptosis. In: Programmed Cell Death, the Biology and Therapeutic Implications of Cell Death. Academic Press, Part B, pp. 107–122. https://doi.org/10.1016/S0076-6879(08)01606-6.
Polazzi, E., Altamira, L.E.P., Eleuteri, S., Barbaro, R., Casadio, C., Contestabile, A., Monti, B., 2009. Neuroprotection of microglial conditioned medium on 6-hydroxy-dopamine-induced neuronal death: role of transforming growth factor beta-2. J. Neurochem. 110, 545–556. https://doi.org/10.1111/j.1471-4159.2009.06117.x.
Qian, S., Wei, Z., Yang, W., Huang, J., Yang, Y., Wang, J., 2022. The role of BCL-2 family proteins in regulating apoptosis and cancer therapy. Front. Oncol. 12 https://doi.org/10.3389/fonc.2022.985363.
Rao, V., Cheruku, S.P., Manandhar, S., Vibhavari, R.J.A., Nandakumar, K., Rao, C.M., Ravichandiran, V., Kumar, N., 2021. Restoring chemo-sensitivity to temozolomide via targeted inhibition of poly (ADP-ribose) polymerase-1 by naringin in glioblastoma. Chem. Pap. 75, 4861–4871. https://doi.org/10.1007/s11696-021-01700-0.
Rayan, A., Raiyn, J., Falah, M., 2017. Nature is the best source of anticancer drugs: indexing natural products for their anticancer bioactivity. PLoS One 12, 1–12.
Rodrigues, T., Reker, D., Schneider, P., Schneider, G., 2016. Counting on natural products for drug design. Nat. Chem. 8, 531–541. https://doi.org/10.1038/nchem.2479.
Rončević, A., Koruga, N., Soldo Koruga, A., Rončević, R., Rotim, T., Šimundić, T., Kretić, D., Perić, M., Turk, T., Štimac, D., 2023. Personalized treatment of glioblastoma: current state and future perspective. Biomedicines 11. https://doi.org/10.3390/biomedicines11061579.
Shamloo, B., Usluer, S., 2019. p21 in cancer research. Cancers 11. https://doi.org/10.3390/cancers11081178.
Singh, S.K., Wang, Y., Habib, A., Priyadarshini, M., Kodavali, C.V., Chen, A., Ma, W., Wang, J., Hameed, N.U.F., Hu, B., Fuller, G.N., Kulich, S.M., Amankulor, N., Colen, R.R., Edwards, L.A., Zinn, P.O., 2023. TP53-PTEN-NF1 depletion in human brain organoids produces a glioma phenotype in vitro. Front. Oncol. 13 https://doi.org/10.3389/fonc.2023.1279806.
Sitarek, P., Toma, M., Ntungwe, E., Kowalczyk, T., Skała, E., Wieczfinska, J., Śliwiński, T., Rijo, P., 2020. Insight the biological activities of selected abietane diterpenes isolated from plectranthus spp. Biomolecules 10, 1–13. https://doi.org/10.3390/biom10020194.
Śliwiński, T., Sitarek, P., Skała, E.M.S., Isca, V., Synowiec, E., Kowalczyk, T., Bijak, M., Rijo, P., 2020. Diterpenoids from Plectranthus spp. as potential chemotherapeutic agents via apoptosis. Pharmaceuticals 13. https://doi.org/10.3390/ph13060123.
Tan, A.C., Ashley, D.M., López, G.Y., Malinzak, M., Friedman, H.S., Khasraw, M., 2020. Management of glioblastoma: state of the art and future directions. CA A Cancer J. Clin. 70, 299–312. https://doi.org/10.3322/caac.21613.
Verhaak, R.G.W., Hoadley, K.A., Purdom, E., Wang, V., Qi, Y., Wilkerson, M.D., Miller, C. R., Ding, L., Golub, T., Mesirov, J.P., Alexe, G., Lawrence, M., O'Kelly, M., Tamayo, P., Weir, B.A., Gabriel, S., Winckler, W., Gupta, S., Jakkula, L., Feiler, H.S., Hodgson, J.G., James, C.D., Sarkaria, J.N., Brennan, C., Kahn, A., Spellman, P.T., Wilson, R.K., Speed, T.P., Gray, J.W., Meyerson, M., Getz, G., Perou, C.M., Hayes, D.

N., 2010. Integrated genomic analysis identifies clinically relevant subtypes of glioblastoma characterized by abnormalities in PDGFRA, IDH1, EGFR, and NF1. Cancer Cell 17, 98–110. https://doi.org/10.1016/j.ccr.2009.12.020.

Wang, F., Gouttia, O.G., Wang, L., Peng, A., 2022. PARP1 upregulation in recurrent oral cancer and treatment resistance. Front. Cell Dev. Biol. 9 https://doi.org/10.3389/fcell.2021.804962.

Wang, Z., Liu, F., Liao, W., Yu, L., Hu, Z., Li, M., Xia, H., 2020. Curcumin suppresses glioblastoma cell proliferation by p-AKT/mTOR pathway and increases the PTEN expression. Arch. Biochem. Biophys. 689, 108412 https://doi.org/10.1016/j.abb.2020.108412.

Warren, C.F.A., Wong-Brown, M.W., Bowden, N.A., 2019. BCL-2 family isoforms in apoptosis and cancer. Cell Death Dis. 10, 177. https://doi.org/10.1038/s41419-019-1407-6.

Weiler, M., Bähr, O., Hohlweg, U., Naumann, U., Rieger, J., Huang, H., Tabatabai, G., Krell, H.W., Ohgaki, H., Weller, M., Wick, W., 2006. BCL-xL: time-dependent dissociation between modulation of apoptosis and invasiveness in human malignant glioma cells. Cell Death Differ. 13, 1156–1169. https://doi.org/10.1038/sj.cdd.4401786.

Wen, P.Y., Packer, R.J., 2021. The 2021 WHO classification of tumors of the central nervous system: clinical implications. Neuro Oncol. 23, 1215–1217. https://doi.org/10.1093/neuonc/noab120.

Yadav, P., Yadav, R., Jain, S., Vaidya, A., 2021. Caspase-3: a primary target for natural and synthetic compounds for cancer therapy. Chem. Biol. Drug Des. 98, 144–165. https://doi.org/10.1111/cbdd.13860.

Yang, W., Chen, X., Li, Y., Guo, S., Wang, Z., Yu, X., 2020. Advances in pharmacological activities of terpenoids. Nat. Prod. Commun. 15, 1934578X20903555 https://doi.org/10.1177/1934578X20903555.

Zhang, Y., Dube, C., Gibert, M., Cruickshanks, N., Wang, B., Coughlan, M., Yang, Y., Setiady, I., Deveau, C., Saoud, K., Grello, C., Oxford, M., Yuan, F., Abounader, R., 2018. The p53 pathway in glioblastoma. Cancers 10. https://doi.org/10.3390/cancers10090297.